Collaborative award Numbers G15AP00012 & G15AP00013

Identification of Faults and Crustal Loads, and their Implications for Intraplate Seismicity in the Northeastern US

Collaborative Research with University of Rochester and Cornell University

Cynthia Ebinger, Department of Earth and Environmental Sciences,
227 Hutchison, University of Rochester, Rochester, NY 14627
cebinger@ur.rochester.edu; 585-276-3364 (phone); 585-244-5689 (fax)

Franklin G. Horowitz, Department of Earth and Atmospheric Sciences,
3134 Snee Hall, Cornell University, Ithaca, NY 14853
frank.horowitz@cornell.edu; 607-255-4829 (phone); 607-254-4780 (fax)

Start date: 12/01/2014; End date: 11/30/2015

Abstract

Intraplate earthquakes in Northeastern North America pose risk to population and infrastructure, yet we remain with few data to differentiate between proposed models for the intraplate seismicity. One testable hypothesis for the location of earthquakes is lateral crustal heterogeneities in the form of composition, rheology, and favorably oriented pre-existing shear zones. Constraints on the location and geometry of faults and lateral density contrasts in crystalline basement beneath the Appalachian foreland basin, Lower St. Lawrence-Adirondacks-Great Meteor Hotspot region, and the Northern Appalachians are foundational elements needed to evaluate the interaction of structures with the tectonic and induced stress fields. Our work primarily evaluated the relationship between crustal structure and earthquake processes in New York, New England, and neighboring areas. We integrated 1) pre-existing seismic catalogues (NEIC); 2) EarthScope TA-derived products with a lower completeness magnitude and better regional coverage; 3) gravity and magnetic survey analyses including Euler deconvolution and multiscale edge wavelet ("worm") analyses; 4) GIS compilation of subsurface structure for calibration of potential fields solutions; and 5) a GIS-based knowledge of population centers and certain kinds of critical at-risk infrastructure such as nuclear power plants. After calibration with known structures, we compared structures identified by Euler deconvolution with worm analyses by analyzing positions of well-located seismic hypocenters with respect to lateral structures detected both by Euler and wavelet methods, and found the that the worms provide superior locations and lateral coverage to the traditional Euler deconvolution technique. We subsequently assumed worms were a good proxy for steeply dipping geological structures, and evaluated their orientation relative to the local SHmax (σ_1) field orientation. Assuming a Mohr-Coulomb failure criterion by slip according to a Byerlee's Law coefficient of friction equal to 0.85, we estimated segments of (worm proxy) structures at orientational risk for seismic activation throughout the region. Our systematic and internally consistent mapping of steeply-dipping lateral contrasts in physical properties of crustal materials across the eastern Great Lakes, St. Lawrence rift and Northern Appalachians results provides a foundation for focused studies and integration with emerging EarthScope data sets. We contribute to the development of a comprehensive understanding of tectonic and earthquake processes by delineating previously unrecognized fault zones associated with earthquakes, or that could be triggered by the release of stress on nearby structures in New York and New England.

1. Introduction

Infrequent intraplate earthquakes in the Northeastern US, which includes 14 urban areas with population > 1,000,000 (http://www.demographia.com/db-ua2000r.htm), pose risk to their population and infrastructure. Causative mechanisms for intraplate earthquakes remain debated largely owing to the limited time scale of historic observations as compared to the stress loading and rapid release cycle (10^2 - 10^4 yr), as well as the lack of constraints on the location, geometry, and kinematics of faults and other zones of weakness that concentrate stress. New challenges arise with industrial activities that may change

the state-of-stress locally, and induce small to moderate earthquakes (e.g., *Ellsworth, 2013*; *National Research Council*, 2013). Intraplate earthquakes may be induced by one or a combination of fluid injection, failure along weak zones after the release of tectonic and post-glacial stress accumulated over time scales > 1000 years, and stress interactions between fault systems (e.g., *Smalley et al.,* 2005; *King et al.,* 1994). While fracturing of intact rock to generate new seismicity is a possibility, the rock record and historic seismicity point to stress concentrations in apparently weak suture zones and pre-existing faults in crystalline basement and steep contacts between zones of strongly varying rheology, such as the multiply-reactivated faults bounding the uplifted Adirondacks mountains (Figs. 1, 2).

The rate of strain accumulation within the elastic plate depends on interior plate stresses, dynamic processes transmitting stresses from beneath the plate, as well as crustal fault geometries, and rheology (e.g., *Bürgmann & Dresen*, 2008; *Freed*, 2005). Thermal and compositional variations strongly influence lithospheric rheology, and consequently, strain distribution (e.g., *Kusznir & Park*, 1987; *Lowry & Perez-Gussinyé*, 2011). Lateral crustal heterogeneities may enhance intra-continental strain localization as indicated by the distribution of intraplate seismicity worldwide (e.g. *Johnston,* 1996; *Newman et al.,* 1999) and from the results of numerical modeling (e.g., *Petit & Ebinger,* 2000; *Lowry & Perez-Gussinyé*, 2012). Knowledge of the location and geometry of major faults within crystalline basement also is needed to evaluate the potential stress triggering effect of nearby fault systems; slip along one fault could increase earthquake risk along nearby faults (e.g., *Freed,* 2005).

Our ability to develop earthquake hazard maps for the Northeastern US, therefore, requires knowledge of the geometry of zones of potential stress concentration within the heterogeneous crust: faults, steep contacts between zones of strongly varying composition, and crustal thickness variations. It also requires knowledge of intraplate stress patterns, and directions in particular, as faults oriented at high angles to principal stress (σ_1) are more likely to be reactivated. and directions. Unfortunately, little is known of the location and geometry of faults, suture zones, or crustal thickness variations beneath sectors of New York, Pennsylvania, and New England. For example, there are few publicly known mapped faults in the Appalachian plateau basin that contains the Marcellus shale, and very little is known of the Grenvillle and northern Appalachian structures in crystalline crust beneath the widespread, up to 10 km-thick Appalachian foreland basin fill (Fig. 2). Yet, the zone of extended Paleozoic crust west of the Appalachians (PEZ), the Adirondack mountain region and the lower St Lawrence rift zone (SLR), and the Northern Appalachian province are some of the most seismically active regions in the Eastern US (Figs. 1, 3). With the deployment of the EarthScope Transportable Array (TA), researchers and earthquake hazard strategists benefit from the improved seismicity detection level and location accuracy. Yet, this 2-year deployment provides a snapshot of the strain accumulation and release process.

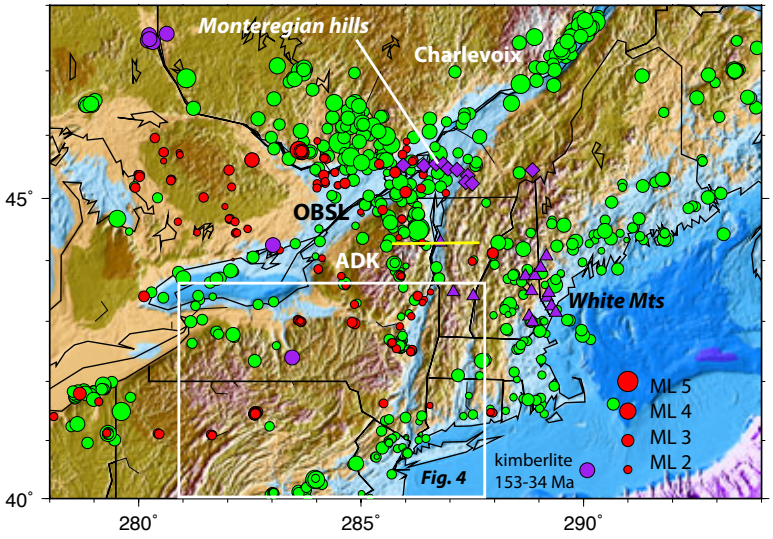

Fig. 1. NEIC earthquake catalogue (green) and 2013-4 earthquakes (red) from Transportable Array. Purple triangles, circles, indicate locations of intrusive and extrusive volcanics (180-100 Ma) as N. America passed over the Great Meteor hotspot; ages young in the ESE direction. OBSL –Ottawa-Bonnechere-St. Lawrence seismogenic zone; ADK- Adirondack seismogenic zone.

The objective of our regional gravity and magnetic anomaly study is to systematically map long-lived

crustal heterogeneities that may serve to localize intraplate strain and magmatism, and to compare the geometry of faults with seismicity and state-of-stress data. We use potential fields data calibrated by new and existing geophysical data, and geological products to identify systematically steep structures and contacts beneath seismogenic zones and throughout the seismically active New England region. Specific objectives are to delineate faults and sutures beneath the Appalachian foreland basin of New York and northern Pennsylvania floored by Paleozoic crust; zones of granitic and mafic intrusions and underplating; and the correlation of these boundaries with intraplate seismicity. We compare and contrast two different spectral methods with gravity and magnetic data: Euler deconvolution and a wavelet-based method referred to as "worms" (Section 3), and we then calibrate inverse model solutions with known faults and steep contacts imaged in independent structural and geophysical data sets. The spatial proximity of earthquake hypocenters in the NEIC catalogue, and the denser but temporary EarthScope catalogue to structures mapped in our study is quantified. These statistics allow us to evaluate the hypothesis that lateral heterogeneities localize strain, and are the sites of intraplate seismicity. In a final section, we highlight steep, potentially seismogenic structures of considerable lateral extent in crystalline basement that lie within a 100 km-radius of large population centers (500,000) or other high-risk infrastructure such as nuclear power plants.

As outlined below, our results identify structures of large lateral and vertical extent that coincide (within errors) with earthquake hypocenters, and similar structures that, by analogy, may be more likely to slip in response to stresses induced by industrial activity (e.g., hydraulic fracturing) and climatically-controlled changes in lake and sealevel. Fluid injection sites may be more susceptible to transient loading by the passage of surface waves from distant earthquakes (e.g. *Kim,* 2013; *van der Elst et al.,* 2013). The new maps of large-scale crustal structures inform earthquake hazard mitigation programs designed to reduce earthquake losses in the US. Where earthquake activity occurs along pre-existing basement structures, particularly where they separate crustal domains with distinct density contrasts, the structures should be prioritized for examination owing to their risk of reactivation. We identify urban areas and nuclear power plants on the Great Lakes and E. Coast in close proximity to large structures showing seismicity (highest priority), morphological evidence for recent movement (high priority), and pre-existing and large-scale geological structures that could be reactivated (priority). This information could be used to inform upgrade of building codes, forward planning, retrofitting infrastructure, and informing local populations and first responders. We expect such forewarning will be beneficial to reducing both financial and injurious losses from earthquakes.

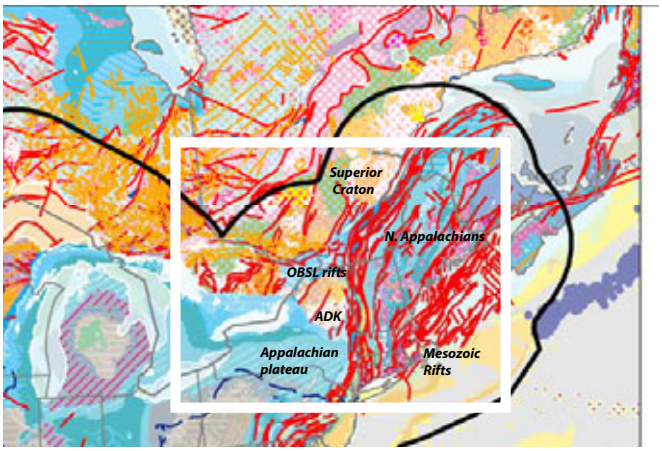

Fig. 2. Study region (white box) within geological context. Red lines are faults. From CEUS-SSC (2012).

2. Tectonic Background

The Grenville (1.6-1 Ga) and Appalachian (0.5-0.3 Ga) orogenic episodes stitched new continental crust and mantle lithosphere to the Superior craton, the core of North America (Fig. 2). Intraplate deformation occurred in parts of the Grenville during the breakup of Rodinia at ~0.6 Ga, and during the collision of Africa and N America to form the Appalachians (e.g., *Whitmeyer & Karlstrom*, 2007). Scars of the breakup of Rodinia in the study area are the Rome trough and the Ottawa-Bonnechère-St Lawrence rifts (Fig. 2). During Mesozoic time, extension initiated along the eastern side of the Appalachians, leading to the onset of seafloor spreading in the N. Atlantic (e.g., *Schlische et al.,* 2003). Between ca. 180 and 100 Ma North America passed over or near the Great Meteor (Monteregian) hotspot track, as marked by a NW-trending track of kimberlitic and alkali volcanism in the Superior craton, Grenville and northern Appalachian zones, and basaltic magmatism along the N England seamount chain (e.g., *Sleep,* 1990;

Heaman & Kjarsgaard, 2000; *Villemaire et al*. 2012; *Kent et al.*, 2016) (Figs. 1, 2). The TA promises to provide critical information on the magmatic and structural modification of crust and mantle lithosphere during this time period of continental rupture along much of the N. Atlantic (e.g., *Schlische et al.,* 2003), but analyses of EarthScope data bases in New England have not yet reached publication stage. The combined effect of these active and ancient orogenic, rifting, and hotspot magmatism episodes have compressed, extended, or added sedimentary and mafic material to the crust of Northeastern North America.

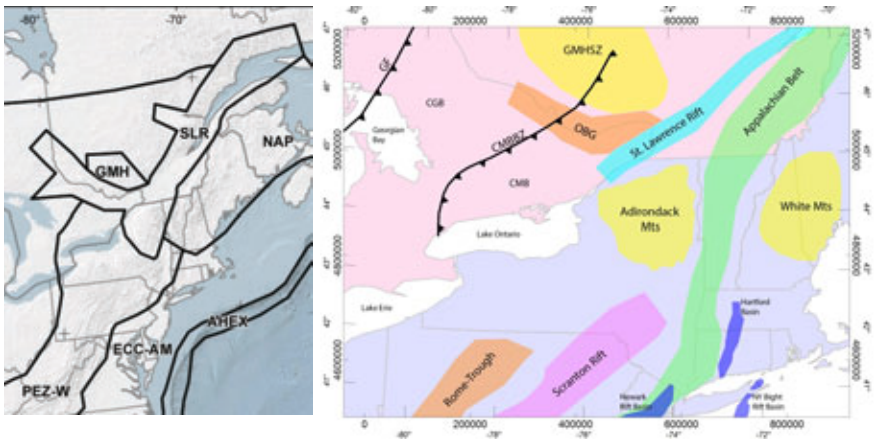

Figure 3. a) Seismogenic provinces from CEUS-SSC (2012). SLR: St. Lawrence Rift, Adirondacks; GMH: Great Meteor hotspot; NAP: N. Appalachian province; PEZ-W: Paleozoic extended crust-wide; ECC-AM: Extended crust–Atlantic Margin. b) Simplified tectonic summary map of Archaean to modern crustal domains and structures. CMBBZ- Central Metasedimentary Belt; OBG- Ottawa-Bonnechère graben; GF: Grenville Front (suture); CGB –Central Granulite Terrain

Rather than duplicate background information on crustal and upper mantle structure summarized in the CEUS-SSC report (2012), we briefly outline constraints on the location and geometry of ancient fault zones, sutures, and intrusives that may remain weak zones and sites of stress concentration in the modern intraplate stress regime. Since some structures extend across seismogenic provinces, we combine the small Great Meteor Hotspot (GMH) seismogenic zone with the St Lawrence Rift (SLR) (Figs. 2, 3). As discussed in Section 5, the CEUS-SSC zonations encompass seismogenic zones, but our studies suggest that causative structures (and perhaps mechanisms) may be better described through different groupings (Fig. 3b).

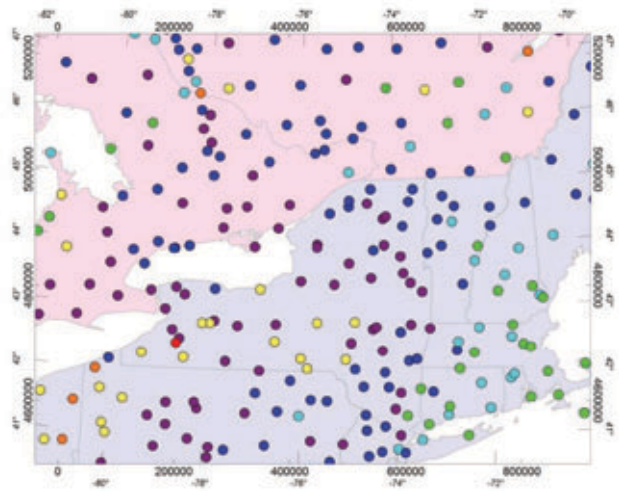

Fig. 4. Crustal thickness estimates from receiver function analyses of EarthScope stations. From *Bahavar & Trabant*, 2010; *Benoit et al.* 2013).

Existing wide-angle reflection and refraction and receiver function data provide constraints on crustal thickness, velocity and fault zones in only a few locations (Figs. 4, 5). A compilation of the existing and publicly available seismic refraction/reflection data and velocity models in Northeastern North America are presented in Figure 5. In particular, there exist COCORP and LITHOPROBE seismic reflection profiles that transect the Grenville orogeny, as outlined in Section 4.4. Confidential industry reflection data exists in some areas, but are unavailable to this study.

2.1 St Lawrence Rift, including Adirondacks (SLR) and Great Meteor Hotspot (GMH)

The St. Lawrence rift and Great Meteor hotspot (Gatineau zone) lie largely within Canada, but ground-shaking from frequent compressional and strike-slip earthquakes along this zone are felt across New England (e.g., *Adams & Basham*, 1991). Grenville-aged basement beneath the Charlevoix zone west of

Maine has been overprinted during Iapetan rifting, Appalachian collision, and by a meteor impact at about 350 Ma (e.g., *Mazzotti & Townend*, 2010)(Figs. 1, 2). Seismicity occurs in two NE-trending bands parallel to the St. Lawrence river, and seismic reflection data reveal an eastward-dipping fault beneath the western zone. The seismic data suggests a large velocity contrast, and hence large density contrast, across this structure (*Vlahovic et al.,* 2003). The NW-trending Ottawa-Bonnechere rift zone is believed to be a failed arm of Iapetan rift zone. A second zone of more diffuse seismicity is associated with intrusives marking the path of the Great Meteor (Monteregian) hotspot, or Gatineau zone (*Mazzotti & Townend*, 2010).

Vintage active-source and magneto-telluric studies across the fault-bounded Adirondacks tectonic block reveal a NW-dipping, high reflectivity, high conductivity lower crust that could indicate the presence of aqueous fluids or residual partial melt (*Brown et al.,* 1983; *Connerney & Kuckes*, 1980), and a high velocity lower crust and uppermost mantle (*Levin et al.,* 1995). Surface wave and body wave mantle tomography studies over local and regional scales image a divot of lower velocity mantle north of the Adirondacks (*Levin et al.,* 1995; *Rondenay et al.,* 2002; *Villemaire et al.,* 2013). Although the low velocity zone and associated Adirondacks uplift has been interpreted as evidence for incipient mantle upwelling (e.g., *Isachsen & Kelley*, 1992), *Villemaire et al.* (2012) interpret these zones as refractory material from melt extraction above the Monteregian/Great Meteor hotspot.

Fig. 5. Seismic reflection and refraction data in Northeastern N. America. See Table 1 in Supplementary material for references to each line.

The Adirondacks is a region of intraplate deformation marked by persistent, occasionally moderate-magnitude seismicity, and active uplift (*Isachsen,* 1975; 1981, *Isachsen & Kelley*, 1992; *Mazzotti et al*., 2005). The cause(s) of the crustal deformation are debated. The Adirondacks region lies within the zone of Glacial Isostatic Adjustment in response to the retreat of the widespread ice load at ~20 Ka. The rate and distribution of vertical and horizontal crustal movements depend on the visco-elastic response of the mantle to the geologically rapid melting of the ice sheet. Geodetic observations document uplift rates of 10 mm/yr in Hudson Bay decreasing to ~3 mm/yr along the US border regions, and with detectable horizontal motions radiating outward from the maximum. *Mazzotti et al.* (2005) suggest that GIA drives crustal deformation within the St Lawrence-Bonnechère regions, with strain concentrations in areas of mechanically weaker lithosphere, including the Sudbury meteor impact zone, and low seismic energy release in areas of stronger lithosphere. Their study did not include the Adirondacks region, owing to sparse geodetic data within the US. Alternatively, the passage of the North American plate over the Great Meteor hot spot in Cretaceous time left crustal heterogeneities in the form of felsic intrusions along the northern margin of the Adirondacks, and in the form of lower velocity zones in the upper mantle (e.g., *Crough*, 1981; *Villemaire et al.,* 2012). *Isachsen & Kelley* (1992) suggest that present-day uplift of the Adirondacks is driven by a new mantle upwelling beneath the Adirondacks, with the high reflectivity, high conductivity lower crust evidence for upward-migrating melt. Some or all of the high relief along the northern margin of the Adirondacks may have been created by rift flank uplift in response to rifting along the Ottawa-Bonnechère rift zones. These areas have experienced $M_L \geq 5$ earthquakes, the cause of which remains poorly understood (e.g., *Ebel & Tuttle*, 2002; *Ma & Eaton*, 2007; *Eaton et al.,* 2005).

2.2 Northern Appalachian Province (NAP)

Current models for the Taconic/Appalachian suture along the eastern margin of the Adirondacks south to the mouth of the Hudson River show west-directed, shallowly-dipping, thin-skinned thrusts and folding above a décollement that overlies and cross-cuts steeply-dipping mid-crustal shear zones (e.g., *Whitmeyer*

& *Karlstrom, 2007*). In addition, geophysical data across the fault-bounded Adirondacks tectonic block reveal strong, sharp lateral heterogeneities in the crust and mantle. However, the complex inter-relationship between thin-skinned and thick-skinned fabrics (e.g. *Hatcher,* 2010) and the implications for reactivation of Rodinian extensional faults during Appalachian orogenesis remain poorly constrained. For example, the fault-bounded margins of the Adirondacks block exhibit evidence for multiple activation / reactivation events, including late Ottawan extension along the western and eastern margins (*Selleck et al.,* 2005; *Wong et al.,* 2012), ancient, possibly re-activated basins of the Ottawa- Bonnechère –St Lawrence rift on the northern and western margins (e.g., *Tremblay et al.*, 2003), and Taconic thrusts and sutures along the eastern margin (e.g., *McLelland et al.,* 2010) (Fig. 2). *Benoit et al*. (2014) use inverse models of Bouguer gravity as well as receiver functions to map lateral variations in crustal composition in the southeastern part of the study area, calibrating results with 2D seismic reflection and refraction data. They find evidence for heavily intruded Proterozoic extensional basins beneath the bend in the Appalachian fold and thrust belt.

2.3 Paleozoic Extended Crust Seismogenic Zone (PEZ-W)

Crustal-scale reflection profiles acquired by COCORP and LITHOPROBE transect the Grenville orogeny, which is largely covered by southeastward-thickening sedimentary strata from the Appalachian foreland basin. Seismic data reveal westward-verging stacked thrust sheets (*Brown et al.,* 1983; *Forsyth et al.,* 1994a,b). Considerable work has been undertaken to map the structure and composition of Grenville and Appalachian fold and fault systems at outcrop, but little is known of the Grenville structures beneath the broad, thick, and largely undeformed sedimentary sequences of the Appalachian basin and Holocene cover (Fig. 2). The high quality deep marine seismic reflection data acquired on Lake Ontario reveal NE-striking faults that accommodated crustal shortening across most of the Central Meta-sedimentary Belt (*Forsyth et al.,* 1994)(Figs. 2, 5). Jacobi (2002) used contoured gravity and magnetic anomaly patterns to suggest fault systems in crystalline basement beneath the Appalachian basin, the lineament analyses provided little 3D information. He identifies N-S, NE, and NW-trending lineaments, some of which have been calibrated against exposed or commercially imaged structures, such as the historically active Clarenden-Linden fault zone (*Jacobi*, 2002). Thus, the subsurface geometry and nature of lineaments beneath the Appalachian basin remained unclear, and the northern extent of the Rome trough remained indeterminate, although *Mazzotti and Townend* (2010) suggest these Iapetan extensional faults continue through western New York to the St. Lawrence rift zone near Ottawa. Northward-increasing glacial isostatic compensation may enhance these differences (*Mazzotti et al.,* 2005; *Sella et al*., 2007).

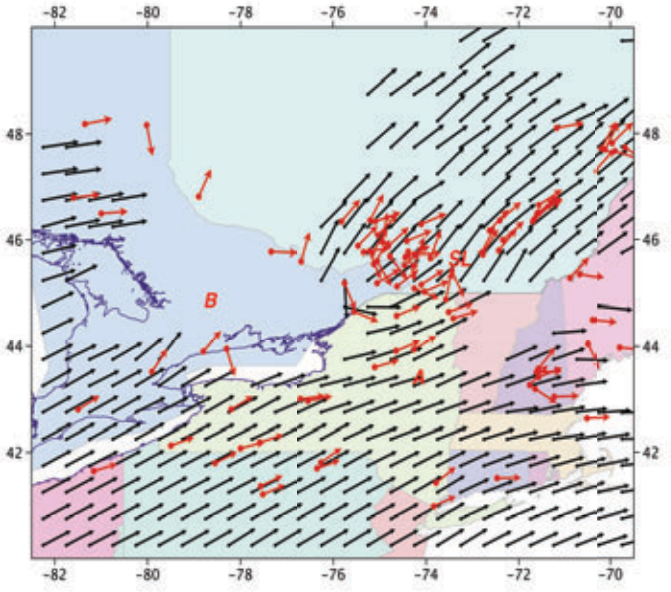

Fig. 6. Extract from World Stress Map (*Heidbach et al. 2010*). Background colors indicate states and provinces. Red arrows indicate direction of high quality S_{Hmax} (σ_1) measurements. Black arrows are a smoothed interpolation on 0.5 degree centers.

Present-day State-of-Stress

The North American plate has remained stable since opening of the North Atlantic, although the glacial loading and unloading have modified state-of-stress within the plate (*Mazzotti & Townend*, 2010). A present day state-of-stress study of this continental intra-plate region reveals deviation in orientation of local stress orientations from regional

stress orientations (*Heidbach et al.,* 2010)(Fig. 6). Specifically, comparisons of the orientation of the maximum horizontal compressive stress (S_{HS}) with that determined from boreholes (S_{HB}) reveal that in the Charlevoix (north of Ottawa-Bonnechère Graben), Lower St. Lawrence rift zone, and Central Virginia zone, the S_{HS} orientation shows a 30°-50° clockwise rotation to the relative regional S_{HB} orientation (*Mazzotti & Townend*, 2010). Similarly, the North Appalachian zone demonstrates similar ~30° clockwise rotation. Possible mechanisms by which consistent local stress perturbations such as these may be generated over large distances is the concentration of post-glacial rebound stresses by local zones of "weakness" and local stress concentrations such as low-friction faults (*Mazzotti & Townend* 2010). Zones of weakness in this case could be locations with variations in crustal composition.

3. Methods

Contrasts in crustal composition and thickness variations cause minute variations within the Earth's gravitational and magnetic field as detected at the surface. Whereas crustal rock densities show relatively small variations, rock magnetic susceptibility may vary by several orders of magnitude. Only crustal rocks above the Curie isotherm (ca. 580°C, lower continental crust) contribute to the crustal magnetic field. Magnetic anomalies, therefore, provide high resolution information on shallow crustal structure, whereas gravity anomalies provide coarser constraints on contrasts throughout the crust (and mantle). Predictive and inverse models of crustal structure can be made that reproduce observed gravity and magnetic signals. Furthermore, fully compiled gravity and aeromagnetic datasets already exist within Northeast North America.

3. 1 Worm' Analyses and Euler Deconvolution

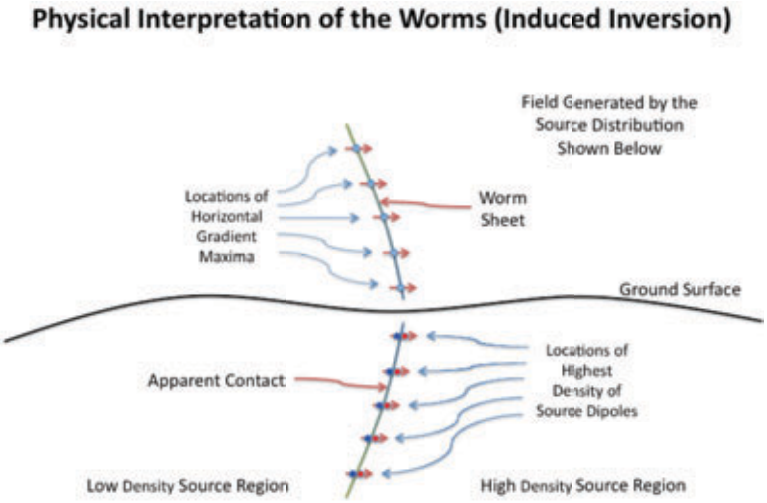

Figure 7. A vertical cross-section cartoon of the worm technique. The gravity or magnetic field is notionally known completely at the ground surface. The field is upward-continued to a suite of heights. *Hornby et al.* (1999) show that each level of upward continuation corresponds to a (continuous) wavelet scale. The locations of maxima in the horizontal gradient of the field at each height become an edge (or a 'worm') for the corresponding scale (the intersection of these 1D features with the plane of section are shown as blue dots above ground), the collection of edges at all scales are 'multiscale edges'. A suite of worms arising from connected locations on the ground is a 'worm sheet'. As explained in the text, an underground inversion is induced via a physical interpretation of the inverse wavelet transform as a distribution of dipole sources. Draping the worm sheets underground (blue and red dots) results in a visualization of the locations of the locally highest density of horizontally oriented dipole sources (*Boschetti et al.*, 2001; *Hornby et al.*, 2002). These are interpreted as the locations of apparent lateral contacts.of dipole sources. These are interpreted as the locations of apparent lateral contacts at depth.

In order to provide a spatially uniform coverage of candidate faults, we turned to the Poisson wavelet multi-scale edge analysis of potential fields – informally known for brevity as the `worm' technique – developed starting nearly 20 years ago: *Hornby et al.* (1999) (independently derived by *Moreau et al.,*

1997). This technique – widely deployed in the mining community in Australia and elsewhere (e.g. GoldCorp, 2001) – uses gravity and magnetic fields to detect lateral contrasts in mass density or magnetization strength respectively. Figure 7 displays a cartoon summary of the technique.

Hornby et al. (1999) show that the magnitude of the horizontal gradient – normalized appropriately to correspond with wavelet theory – changes amplitude with upward continuation/scale-change in such a fashion as to identify the Lipschitz exponent (related to the fractal dimension) of the underlying singularity in the source distribution. That is, if we define

$$M(x,y,z) = (z/z_0) \; || \; (\partial_x + \partial_y) f(x,y,z) \; || \qquad (1)$$

where ∂_x and ∂_y are (vector-valued) gradient operators in the x and y directions respectively, $||\bullet||$ denotes the Euclidean length of the vector sum, and $f(x,y,z)$ is our potential field as a scalar function of height and lateral position (e.g. $f = ||g_z||$ for gravity surveys, or f = pseudogravity for magnetic surveys) then $\partial M / \partial z$ is the quantity of interest in determining the Lipschitz exponent. M is often displayed as the worm color, and one can visually assess $\partial M / \partial z$ from the graphical representation. The Lipschitz exponent concept is closely related to the geophysically-more-widely-known 'structural index' from Euler deconvolution (e.g. *Reid et al.,* 1990). A masters thesis (*Navarrete,* 2015), as well as work by *Carpenter et al.* (2015) shows that the locations of worms and Euler solution routinely coincide, but that the worm technique offers significantly enhanced lateral coverage over the Euler deconvolution solutions as well as better proximity statistics to recorded earthquakes, as we discuss in 5.3 and 5.4 below.

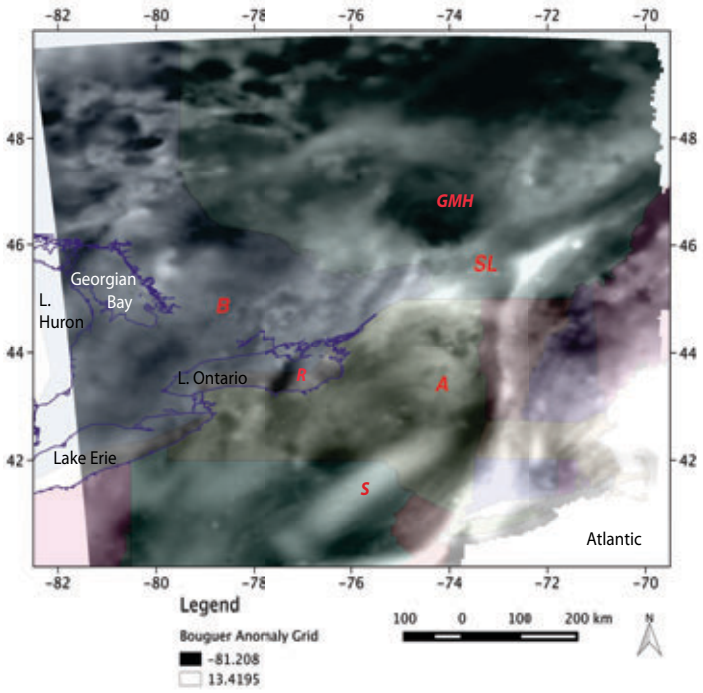

Fig. 8. Bouguer gravity anomaly data from N. American data base. SL: St Lawrence; A: Adirondack block; GMH: Great Meteor hotspot; R: Rochester basin; S: Scranton anomaly/Proterozoic rift zone; B: PEC-W seismogenic province. Data points in Supplementary Materials Fig. 1.

The result is highly interpretable (e.g. *Jessell,* 2001) preserving the strike, the sense-of-dip, and geometric information traditionally captured by Euler poles. However, by virtue of the inverted distribution of rock surfaces gets smoother with depth, the source distribution at depth is poorly constrained. In these analyses, all fields were pre-processed to Bouguer or pseudo-gravity using the commercial software OASIS/Montaj. The worm analysis was then be performed on the gravity and pseudo-gravity fields (e.g., Figs. 8, 10)

4. Data

Due to their relatively low cost of acquisition, gravity and magnetic data provide regional-scale coverage at a sampling density that is unavailable with subsurface imaging data sets. Tests of models come from independent data sets, such as seismic reflection profiles and receiver functions. Using the results of the potential field analyses and constraints from available geophysical data, geologically plausible models of crustal structure can be created and tested using forward models.

4.1 North American Gravity Database

We use the North American Gravity Database, which utilizes modified reduction procedures to minimize error in regards to terrain, Earth curvature, second-order vertical gradients in gravity, atmospheric mass effects, and differences in the normal gravity and station height datums (*Hinze et al.,* 2005). Resultant

Bouguer gravity anomalies are representative of gravitational acceleration due to sub-sea-level density contrasts, although small amplitude anomalies associated with lateral density variations in the crust above sealevel may be mapped to the subsurface. On the other hand, Bouguer anomalies are less sensitive to acquisition errors in elevation, the largest source of error (e.g., *Blakely,* 2006). Prior to analyses, the dataset was converted into the standard UTM zone 18 projection in order to have constant grid spatial separation for spectral analysis. A grid cell size of 2.5 km was used to remain consistent with the coverage of the dataset in Northeastern North America.

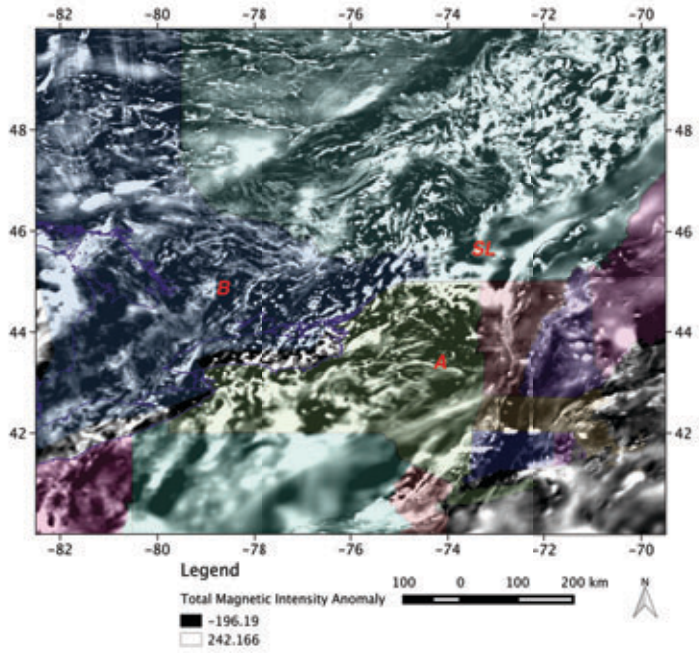

Fig. 9. Total magnetic intensity map from NAMAM2008 (in nT). SL: St Lawrence; A: Adirondack block; B: Grenville province affected by rifting in Paleozoic.

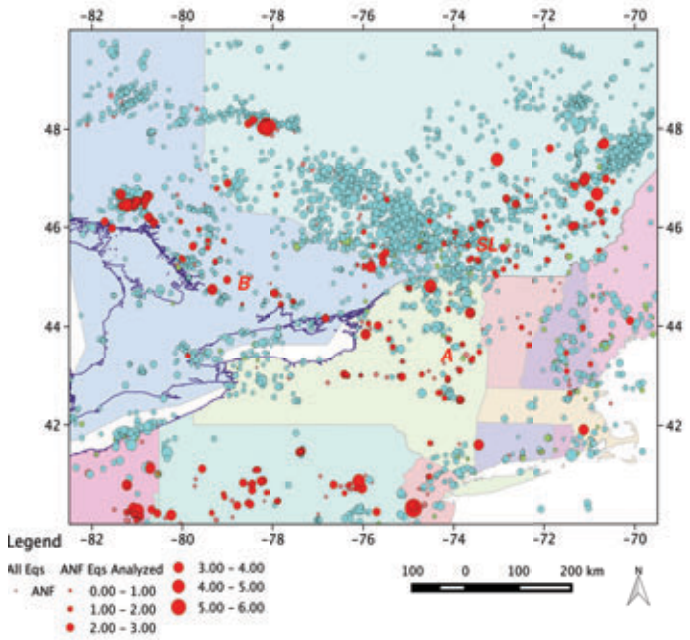

Fig. 10. Seismicity data from NEIC and ANF catalogues. SL: St Lawrence; A: Adirondack block; B: PEC-W seismogenic province. All events in light blue. Well-located events in red were selected for statistical comparison with worm and Euler solution locations.

4.2 Magnetic Anomaly Database

A combined grid of the National Uranium Resource Evaluation and the North American Magnetic Anomaly Map (NURE-NAMAM2008) (*Ravat et al. 2008, 2009*), a regional reduced-to-the-pole magnetic anomaly compilation, was utilized. The NURE-NAMAM grid was converted into the standard UTM zone 18 projection with a grid cell size of 1.25 km (Fig. 9). Magnetic dipole anomaly patterns are skewed by latitude-dependent magnetic inclination. We transform magnetic anomalies to pseudo-gravity (monopole) anomalies (e.g. *Blakely*, 1996; equivalent to reduced to pole total field magnetic anomalies followed by vertical integration then scaled to gravity amplitudes) prior to wavelet analyses to enable direct comparison with gravity anomaly solutions (Fig. SM2). Due to the wide variability between magnetic susceptibility values for the same lithology, these readings were used to create range values for our predictive models (*Muir* 2013).

4.3 Seismicity

We use the NEIC database and the earthquake data base prepared by the EarthScope Array National Facility (ANF), which includes location and depth errors. This database may include quarry blasts and other industrial activity which is hard to

detect without re-analyses of waveforms. We could have removed all earthquakes that occurred between 08:00 and 18:00 local time as a best guess for the US events – due to regulatory restriction of blasts to daylight hours, but we have no information about timing of industrial activity throughout the Canadian region.

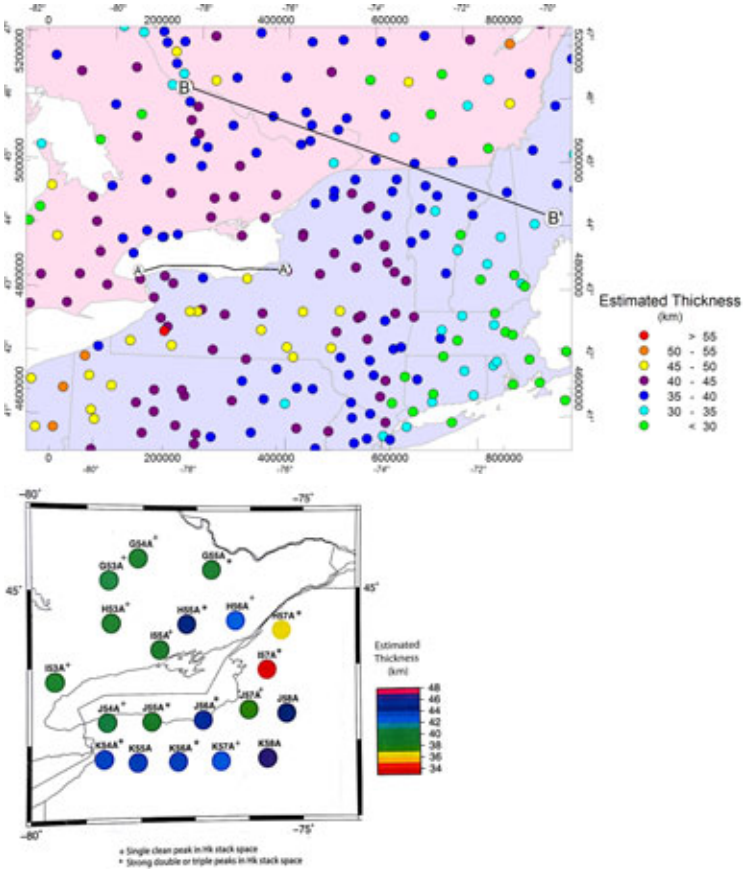

Fig. 11. **A)** Crustal thickness estimates from automated receiver function processing of TA stations (*Bahavar & Trabant* 2010). Crustal thickness estimates are displayed as circles divided into color ranges . Lines A-A', B-B' denote locations of predictive models of crustal structure designed to calibrate Euler and worm results (Figs. SM3, SM4). **B)** Re-analyses of automated receiver function analyses (M. Benoit, pers. Comm. 2014)

4.4 Crustal Thickness Constraints

Automated receiver function results from transportable array EarthScope stations were used (*Bahavar & Trabant,* 2010) (Figs. 4, 11). In the PEC-W zone, collaborator Margaret Benoit re-analyzed data from five TA stations south of Lake Ontario where reflection data exist, and where we calibrate solutions (Figs. 4, 11). Given the sparse coverage by seismic reflection and refraction datasets, we focus efforts on two long profiles of crustal structure, and use these independent datasets to calibrate and test inverse models. Structural patterns observed along a vintage seismic reflection line from *Forsyth et al.* (1994a) provide subsurface constraints on crustal structure with which to calibrate our Lake Ontario predictive model. The 24-Fold stacked and migrated data were acquired using a marine vibroseis source (*Forsyth et al.*, 1994a). The 1971 line images reflections as deep as 10s (30-35 km), ideal for the crustal-scale targets of this study. Additionally, a composite 650 km-long crustal velocity model was used to calibrate the Northeast North America transect predictive model (*Hughes & Luetgert*, 1991, 1992; *Musacchio et al.* 1997)(Fig. 4). This profile crosses perpendicular to the strike of the Grenville thrusts exposed in southern Ontario and the Adirondack Mountains, and structures in the New England Appalachians. The resulting P-wave velocity models can be compared with known quantitative relations between Vp and density to derive appropriate density values for the crust (e.g. *Brocher* 2005). This velocity model is used to test our Grenville-Appalachian transect predictive model. Specifically, P-wave velocities from the velocity models presented in *Hughes & Luetgert* (1991, 1992) were compared with P-wave to density relations presented in *Brocher et al.* (2005). This allowed us to estimate density constraints for our 2D predictive model that tests inverse model results.

5. Results

Euler deconvolution and multi-scale edge analyses (worms) analyses together provide bounds on the depth extent of step-like structures separating domains with differing physical properties.

5.1 Euler Deconvolution – Gravity and Magnetic Anomalies

The results from our Euler deconvolution analyses of both gravity and magnetic anomalies reveal depth and geometry of subsurface density and magnetic susceptibility contrasts (Figs. 12, 13). We aim to locate step-like structures of large lateral extent and depths greater than 5 km, so we use a depth-scaling relationship appropriate for steep structures: a structural index of 0.5 (e.g., Reid et al., 1990). For this reason we will only interpret solutions that are focused, and hence, satisfy the assumption of steep structures. Focused solutions are Euler solutions that are clustered together and are positioned in alignment with nearby solutions indicating that they are indeed step-like, as opposed to cylindrical or circular structures. Thus, unfocused solutions appear spread out or unaligned and are not interpreted (Fig. 14).

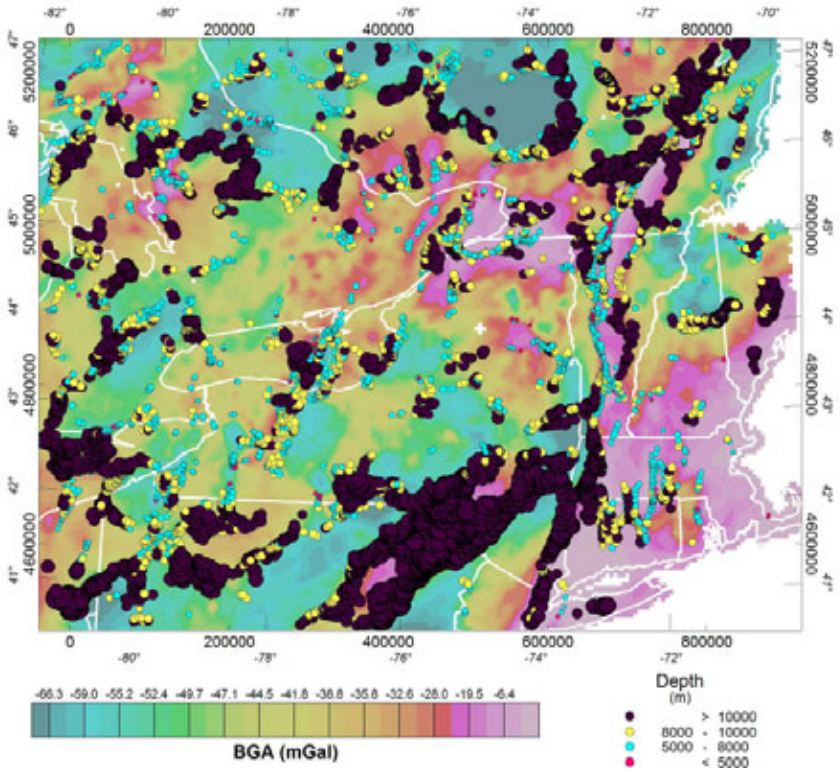

Fig. 12. Bouguer anomaly Euler deconvolution results, with size and color proportional to depth below surface. Clusters of BGA solutions are observed throughout the Grenville Province (including Adirondack Mts), Appalachian Mountain Belt, Monteregian Hills-White Mountains-New England Seamounts volcanic chain, and Proterozoic, Paleozoic and Mesozoic rift basins (Fig. 14).

SLR-GMH

In the Ottawa-Bonnechère Graben, St. Lawrence Rift, and Great Meteor Hotspot Seismic Zone, we observe close clusters of solutions suggesting steep structure at mid-crustal levels.

PEZ-W

Throughout the Appalachian basin we observe N-S and NNE-trending lineaments of Euler solutions, suggesting steep structure extending below the Paleozoic cover of the area. Examples are the N-S trending chains of solutions beneath Lake Ontario, and solutions to mid-crustal levels beneath the Central Gneiss and Fig. 13. Magnetic anomaly Euler deconvolution results (purple) overlain by earthquakes at depths less than 15 km. The increasing depth to solutions in the St. Lawrence, Appalachian, and extended Atlantic Margin area is a consequence of basement burial by thick piles sedimentary rocks with weak magnetic susceptibility. Central Meta-sedimentary Belt, Georgian Bay, and eastern Lake Erie (Figs. 12-14). These solutions range from ~5km to >10 km. Euler deconvolution results for the magnetic anomaly grids show many shallow solutions in areas of exposed metamorphic basement, but solutions deepen with increasing depth of burial beneath the Appalachian Foreland basin, and along the US East Coast passive margin.

NAP

Northern Appalachian Province Euler solutions occur along the length of the belt, and extend from surface to lower crust (Fig. 14-16). Notable are the two sub-parallel bands of deep solutions along the northern Appalachians, whereas the central Appalachians are marked by a single, crustal-scale line of solutions. Within the White Mountains we observe closely-spaced solutions implying steep, near vertical, density contrasts near edges of intrusives.

ECC-AM

Within the Mesozoic rift basins east of the Appalachian Belt we observe deep solutions that correlate with large offset border faults and intrusives in Mesozoic rift basins. An example is the N-S striking line of solutions marking the Hartford basin, and other Mesozoic East Coast rift basins.

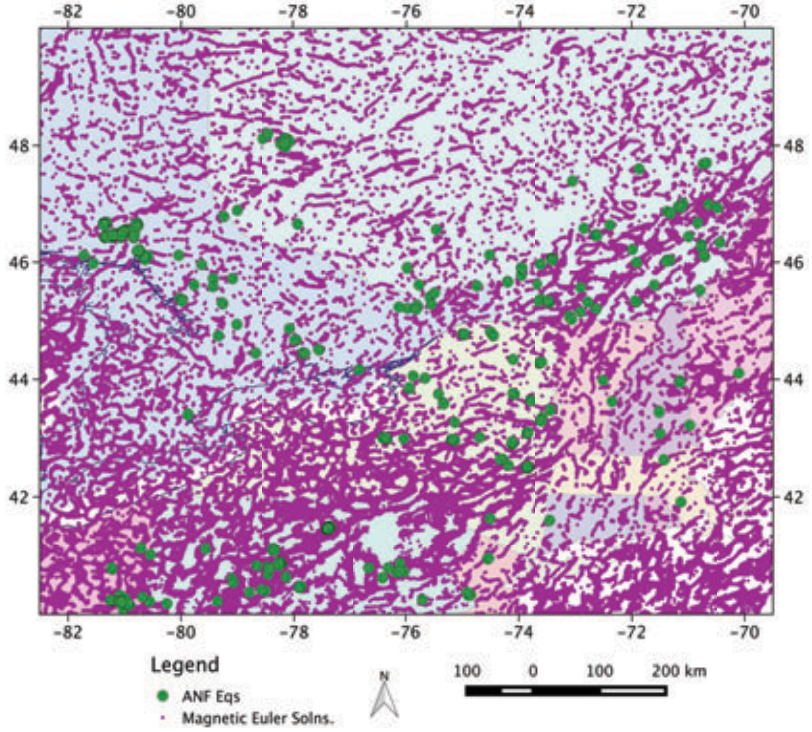

Figure 13. Magnetic anomaly Euler deconvolution solutions (purple) overlain by earthquakes (green) with depths <15 km. Most solutions are < 7 km, although depths increase to >10 km beneath the Appalachian basin and East Coast passive margin sedimentary basins.

5.2 Inverse wavelet transform

The worm results for this project are calculated by open-source code described in *Horowitz & Gaede* (2014). A git repository of that code may be found at <https://bitbucket.org/fghorow/bsdwormer> with its complete revision history. The results for the 'worm' analyses reveal the locations and geometry of lateral contrasts in density and magnetic susceptibility (Figs. 15, 16, Section 6). While such structures are clearly candidate faults, not all worms are faults (consider dipping beds), and not all faults have worm signatures – perhaps due to no material property contrasts being created by the faulting. However, we argue that even if such structures are inactive at present, simply by having mechanical properties be correlated with mass or magnetization density, structures identified by worms are good candidates for reactivation. This idea underpins one estimate of risk for *induced* seismicity for prospective industrial operations in the Appalachian Basin (*Horowitz et al.,* 2016).

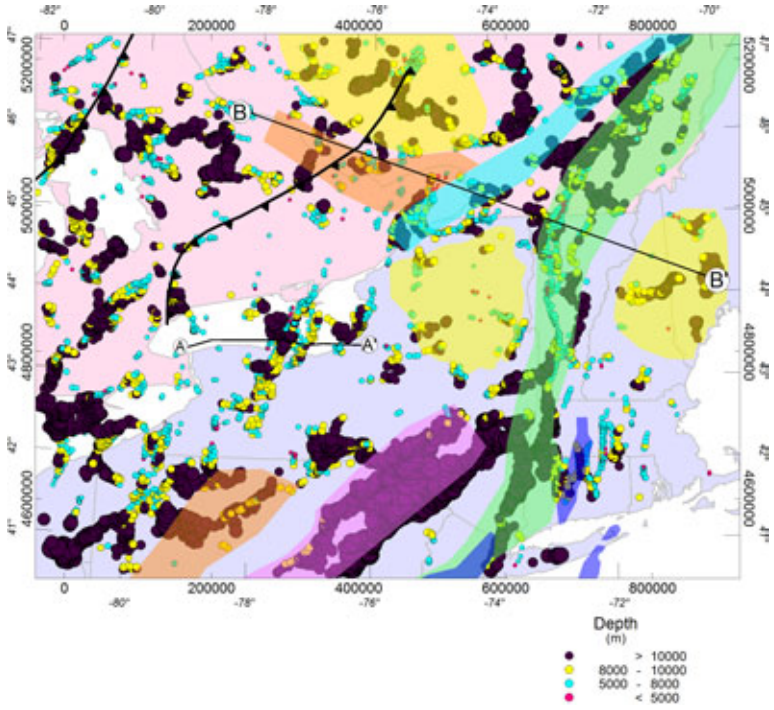

Fig. 14. Simplified geological map from Fig. 3 on BGA Euler solutions. We use Euler solutions for simplicity, since they show major features, but worm solutions are preferred. Colored circles indicate the locations of Euler solutions whose size are scaled with depth. B-B' marks the location of our Northeast North America predictive model. A-A' marks the location of our Lake Ontario predictive models (Figs. SM 3, 4).

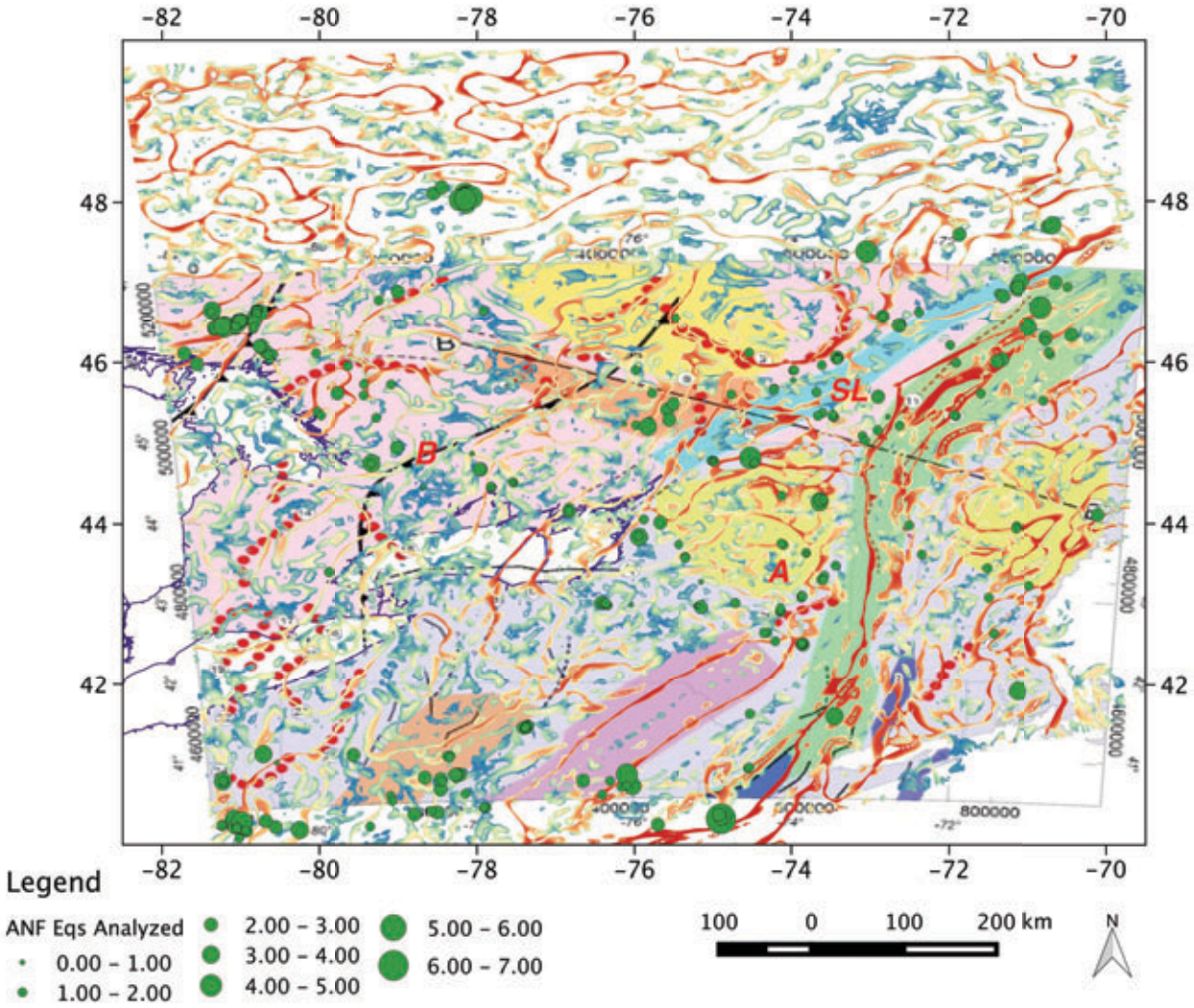

Figure 15. Worms for Bouguer gravity anomalies from a 15 to 1 km depth range. Colored by rainbow spectrum of log_10 (wavelet scaled magnitude) of horizontal gravity gradient with blue = -4.57 log (scaled gravity units/meter) — low; ranging to red = -1.45 — high. Note the sharp chains of worms along the eastern edge of the Adirondacks (A), along the St. Lawrence (SL) seismogenic zone and the Charlevoix seismic zone (Figs. 1, 3). The simplified map of Fig. 3b is included for reference.

5.3 Comparison between inverse models

Although the full comparison is not presented, we used geospatial analyses to determine all solution sets that were coincident in 1) Bouguer worms and Bouguer Euler results; 2) Bouguer Euler and PGA Euler; 3) Bouguer worms and PGA worms; 4) PGA Euler and PGA worms. All of the Bouguer and PGA Euler solutions have corresponding worm solutions, but not vice versa. All of the Euler magnetic anomaly solutions have corresponding PGA worm solutions, but not vice versa. The Euler solutions are more discontinuous, and the comparison indicates that the Euler method loses detail and continuity owing to the large window size utilized to constrain deep sources.

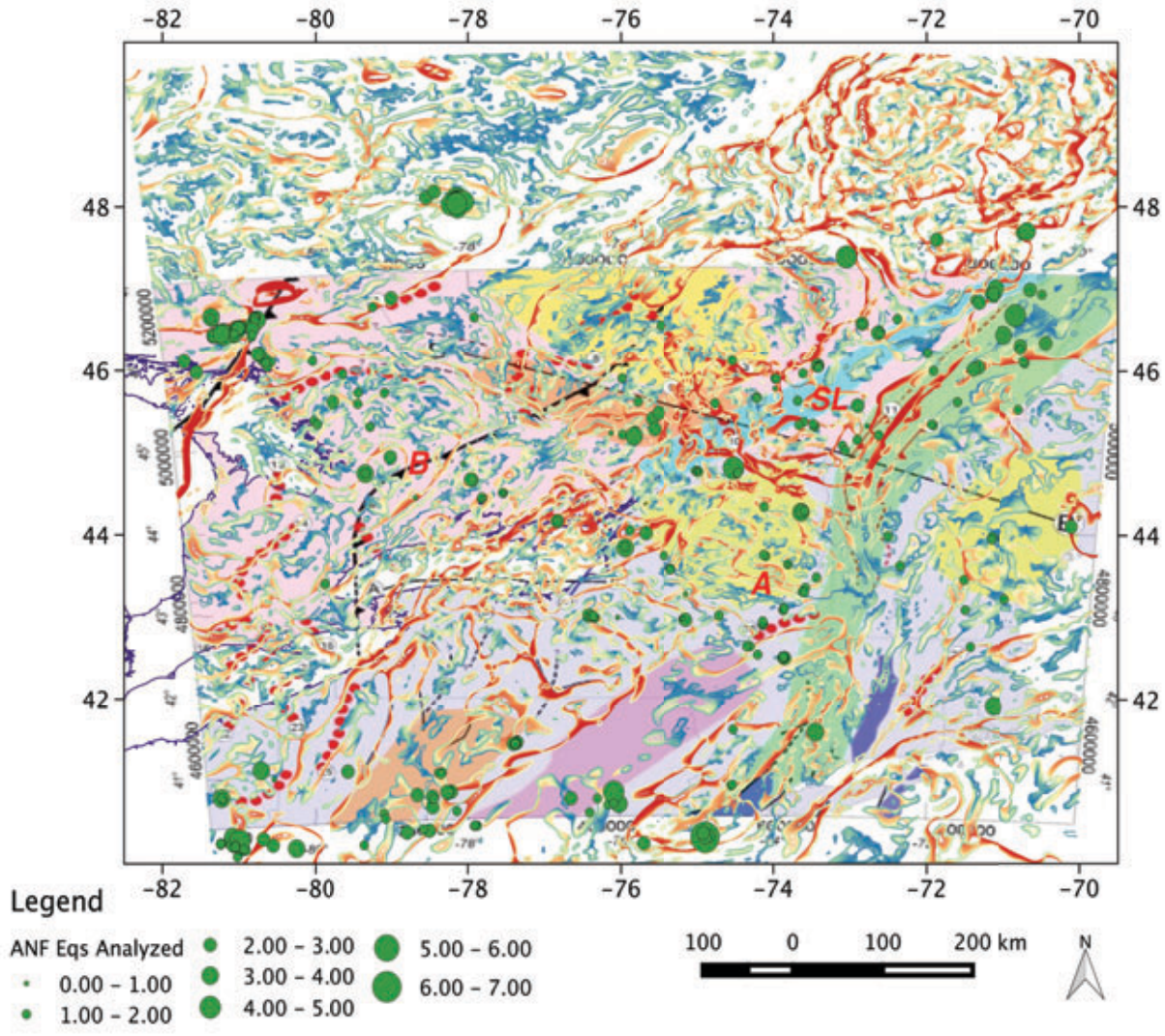

Figure 16. Worms for pseudo-gravity anomalies (e.g. *Blakely*, 1996). Colored by rainbow spectrum of log_10(wavelet scaled magnitude) of horizontal pseudo-gravity gradient with blue = -6.32 log(scaled pseudo-gravity units/meter) — low; ranging to red = -2.79 — high. Whereas our BGA results (Fig. 15) – due to their coarser underlying grid – provide strong constraints on mid- to lower crust (depths > 8 km), these pseudo-gravity worms – due to a grid with ½ the pixel size – are sensitive to shallow contacts, sutures, and lithological boundaries. The simplified map of Fig. 3b is included for reference.

Comparison of depth extent of solutions, and our ability to resolve dip of structures does, however, vary between methods. In both methods, depth is constrained by the wavelength and amplitude of anomalies, and signal amplitudes decay with depth. Both methods lead to vertical smearing of solution depths at the limits of resolution. These effects are clear in the two geological cross-sections constrained by seismic data (Figs. SM3, SM4). The corresponding forward models also are insensitive to small changes in the dips of contacts in the lower crust. Based on these comparisons, we restrict displays to solution depths < 15 km. Only locations with coinciding BGA and magnetic Euler results also coinciding with strong contrasts imaged by the 'worms' are interpreted as deep structures within the region (Fig. 17). Where structures have shallower dips, the worms produces solutions clustered on the updip section, whereas the Euler solutions cluster downdip, as along the Grenville thrust sheets imaged beneath Lake Ontario.

5.4 Comparison with Seismicity Distribution

We compare earthquake distribution and depth with respect to each of the structures and steep contacts identified in these studies. We rely on a recent study of state-of-stress throughout the region by Mazzotti and Townend (2010) because only a few new focal mechanisms are available, and no updating is necessary. Figures 13, 15-16 provide a spatial comparison of worms and epicenters, but a full 3D comparison of hypocenters and Euler and worm solutions is required to evaluate proximity. Figure 18 is a histogram of occurrences of earthquakes and BGA and PGA worm points and earthquake epicenters, with consideration of errors in both. These results demonstrate that more than 20 percent of well-located earthquakes in the region lie within location precision of a worm point. Given that large parts of the area are aseismic, this result allows us to interpret some worms as active faults, and hence focus on worms as

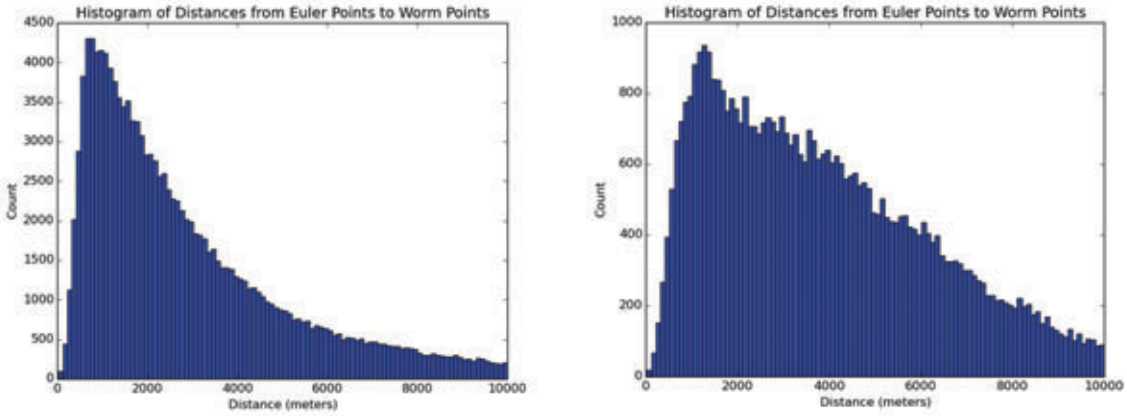

Figure 17a, b. Comparison of distances between a) Pseudo-Gravity magnetic worms and Euler solutions and b) Bouguer Euler solutions and worms. Supplementary Material provides spatial comparisons, and illustrates the close correspondence between structures of large lateral extent throughout the region. In effect, all of the Euler solutions have corresponding worm solutions, but the worms provide better continuity and higher resolution imaging. The largest discrepancies occur at depth, and reflect weak dip constraints in smooth potential fields data.

locations that might either potentially be activated in the future or be candidate locations for induced seismicity.

5.5 Calibration

We calibrate our results with known Appalachian basin and basement fault zones. Specifically, we observe NW and NS striking solutions along the Rome-Trough, the Keuka fault zone, and deep solutions along the borders of the Scranton Rift (*Benoit et al*. 2014; *Jacobi,* 2002). To the southeast, along Mesozoic rift basins, we observe deep solutions correlated with previously known faults, and locations of thrusts of the Appalachian belt (*Benoit et al.* 2014; *Withjack* 1998; *Whitmeyer & Karlstrom*, 2007). Simplified crustal-scale geological cross sections along the sparse seismic reflection and refraction profiles where velocity data provide independent constraints on subsurface density provide independent methods to compare and contrast Euler and wavelet results, and to calibrate solutions (Figs. SM3, SM24). We ignore shallow and poorly-constrained structures which are beyond the aims of this study. This . calibration work was a core component of the MSc thesis by *Navarrete* (2015). Forward models of potential field anomalies are non-unique, but they are useful for visualization and testing, where independent crustal constraints are available, as along Profiles A-A' and B-B' (Figs. 11, 21).

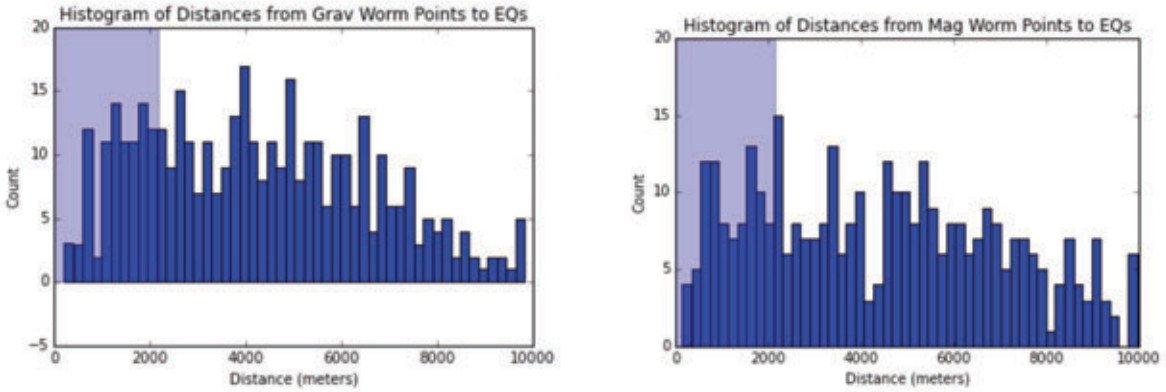

Figure 18. Histogram of earthquakes occurring within 5 km distance from a) BGA worm solutions and b) pseudo-gravity (magnetic anomaly transformation). Blue shading indicates earthquakes that coincide with worm points, considering errors in earthquake and worm locations. To produce these histograms, the closest gravity or magnetic worm point (of ~500,000) to each well-located earthquake was found via a custom coded spatial proximity query, and the distance histograms are plotted above. Then, hypocenter location error statistics were estimated and combined with worm location error estimates to produce the blue shaded "within error" zones at the left of each histogram. Work completed as senior thesis by K. Carpenter, Rochester undergraduate.

5.6 State-of-Stress Direction Comparison

Figure 19 demonstrates a first-principles solid mechanics viewpoint on structural orientation as determined by planes defined by worm orientations with respect to the regional stress field, and their potential for failure. We display some relevant Mohr's circles along with both Byerlee's Law (*Byerlee*, 1978) and Griffith-Coulomb failure envelopes. In those Mohr-space figures, two planes best oriented for failure by Byerlee's Law are marked with red dots. (There are two additional symmetrical orientations in the lower half of the Mohr diagram not shown for visual simplicity.) The angle a candidate plane normal makes from σ_1 (max principal stress) appears to be a sensitive parameter for proximity to failure under a Mohr-Coulomb failure model.

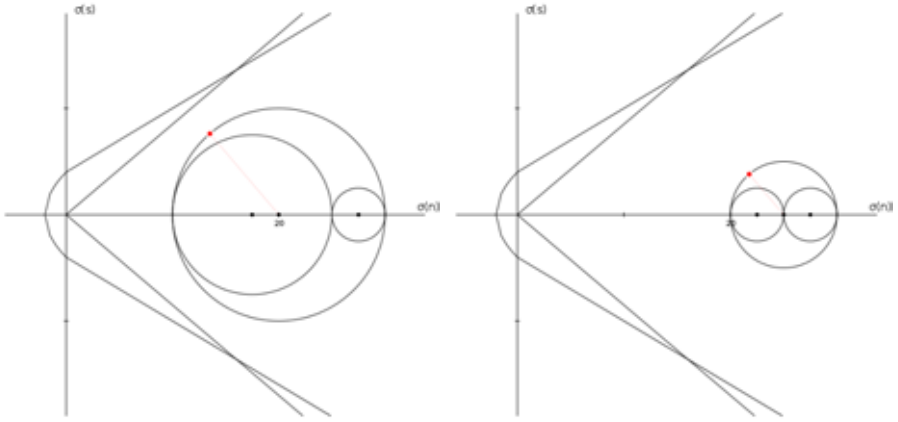

Figure 19. Shown in (a) are 3D Mohr's circles for notional principal stresses of 30, 25, and 10 MPa, along with failure envelopes for both pre-existing fractures (Byerlee's Law – straight line envelope; coefficient of friction $\mu = 0.85$ and zero cohesion) and failure of intact rock (Griffith- Coulomb criterion – curved envelope). Similarly for (b), but with a different value of $\sigma_3 = 20$ MPa resulting in a significantly further from failure situation. In both plots, the poles of one orientation of the closest-to-failure planes are plotted as a red dot on the circumference of the outer (σ_1–σ_3 plane) circle. The angles of poles to the closest-to- failure plane are identical in the two situations even though (b) is less risky than (a) because its red dot is further away from a failure envelope. Plotted using R. Allmendinger's MohrPlotter software.

One major caveat: that orientation-in-a-regional-stress-field metric holds true wherever the actual state of stress is known (i.e. where the radii of the Mohr's Circles in Figure 19 are established). In our situation however, we have very little information about the magnitudes of the principal stresses – other

than the trivial vertical lithostatic case due to burial depth and ρgh. An unavoidable consequence of that fact is that any risk estimates we make using this technique are **local only**. Local changes in risk nearby along worm segments should be qualitatively captured – assuming locally smooth changes in stress magnitudes. However, quantitatively comparing the seismic risk factor from one location to another location at some distance removed **is not feasible** because the unknown stress magnitudes also play a role not captured by orientation. Hence, segments identified as possessing the same 'risk factor' using this

technique will unavoidably have different quantitative risks of seismicity. Another way of saying the this is that planes with poles nearly normal to the Byerlee's Law envelope in both (a) and (b) of Figure 19 will be estimated to have the same risk using this technique, even though the situation in Figure 19 (a) is significantly closer to failure.

As described in *Horowitz et al.* (2016), an orientation statistical approach (derived from *Mardia*, 1972) and regional stress field orientation interpolation (using the technique of *Heidbach et al*., 2010) are used to estimate a risk for seismicity at each point along a worm. Briefly, the worm orientation is estimated at worm points, and its normal direction for an assumed vertical dip is compared with the SHmax (σ_1) orientation there. Worms within a 5° mis-orientation in real space (10° in Mohr space) are categorized as highest risk, within an additional 5° as a moderately high risk, within another 5° as a moderate risk, and all other worm points – simply because they are on an identified structure – are categorized as a moderately low risk (Fig. 20). The geologically short time period of seismicity observations compromises tests of these hypotheses.

6. Interpretations

Locations where the gravity, magnetic, and pseudo-gravity Euler deconvolution and 'worms' coincide are interpreted as structures of deep extent. The results from our comparison are separated into four separate result categories in decreasing order of confidence: 1) Known structures that are well imaged throughout the region, 2) Continuations of known structures, 3) New structures of deep extent calibrated by surface data, and 4) New structures similar to imaged structures but that lack any subsurface data. Figure 21 below summarizes potential field solutions that correspond to known structures, and identifies similar patterns that are also interpreted as major crustal-scale faults and sutures. Many more structures may be identified after detailed analyses of state reports, detailed maps, and theses, but thses comparisons are outside the scope of this study. We focused our calibrations on two areas: the seismogenic regions of western New York where Paleozoic Rome trough structures may underlie the Appalachian basin and Lake Ontario, and the known seismically active fault zones of the Adirondacks and Northern Appalachians. Patterns along the East Coast underlain by Mesozoic extensional structures require further detailed analyses.

6.1 SLR-GMH

Euler and worm solutions within the area affected by the Great Meteor hotspot and Ottawa-Bonnechère rift zone show several orientations. NW-striking solutions match the known orientation of steep faults bounding the Ottawa-Bonnechère rift zone, based on subsurface data from *Mereu et al.* (1986). Another prominent anomaly '4' on Figure 21, has a NNE-N-S orientation. Solutions within the St Lawrence rift and seismogenic zone have NE-orientation, parallel to known active faults, and consistent with state-of-stress information (Fig. 6). Elliptical solutions appear to intersect the NE-trending St. Lawrence rift structures in some areas.

6.2 NAP

Euler and worm solutions show a range of orientations, with the most prominent crustal-scale structures associated with northern Appalachians thrust faults that are steep at the surface, and that juxtapose high-grade metamorphic rocks with lower-density rocks. An example is the Grenville Ramp (Champlain thrust)(11 on Fig 23). Elliptical clusters of solutions correspond to the known Mesozoic intrusives of the Great Meteor hotspot, including an exposed stock near number 12 on Figure 21 (*Ratcliffe et al.,* 2011).

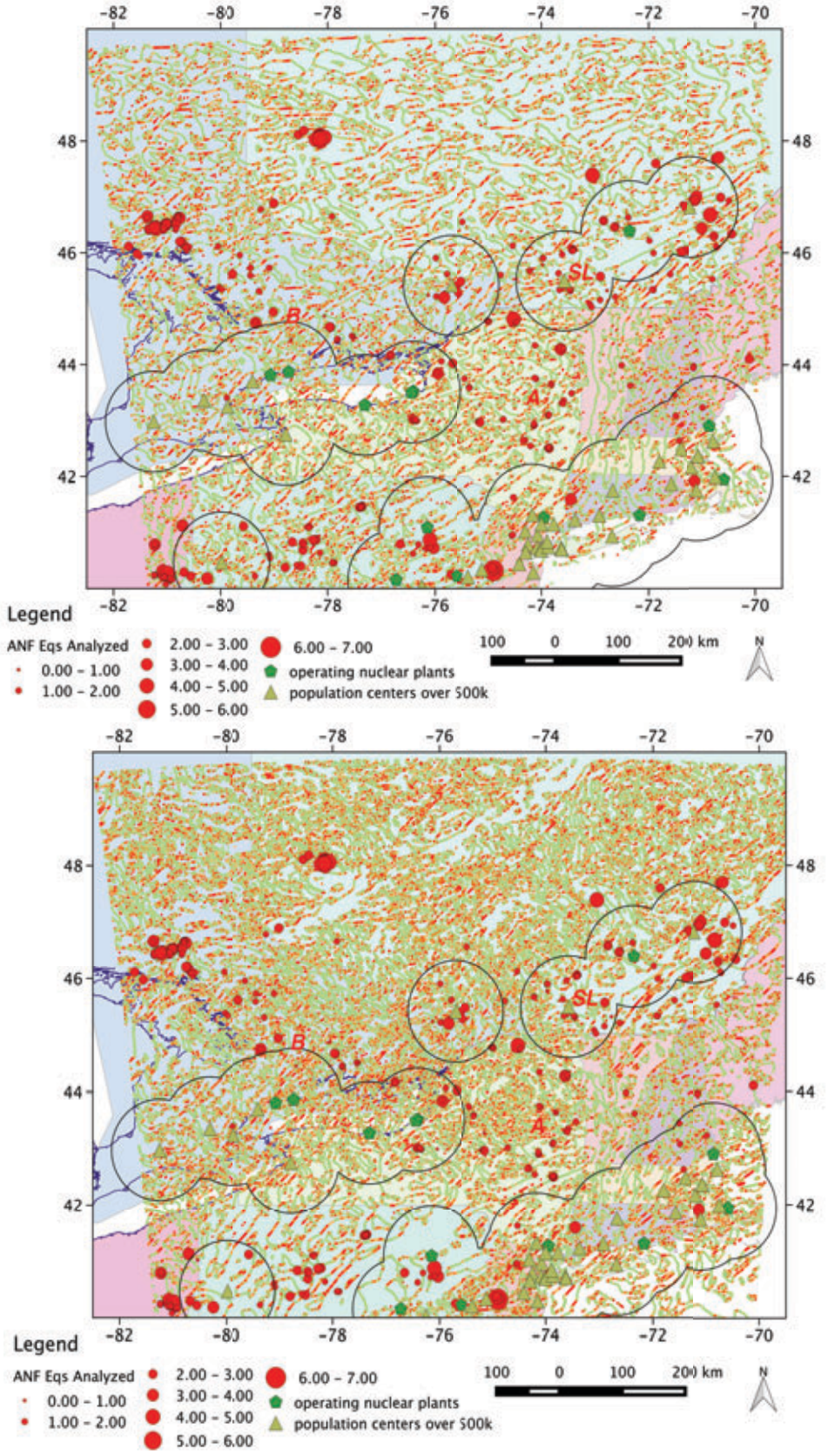

Figure 20. Misorientation of worms from gravity (top) and magnetic pseudo-gravity (bottom) fields in the regional stress field. The risks are categorized by 5° misorientation increments to a critical stress orientation for a Byerlee's Law (μ= 0.85) failure criterion. The stress field orientation is interpolated using the technique described in *Heidbach et al.* (2010).

Also plotted are locations of population centers >500,000 and operating nuclear plants, with a 100km buffer zone surrounding them. See text for more details.

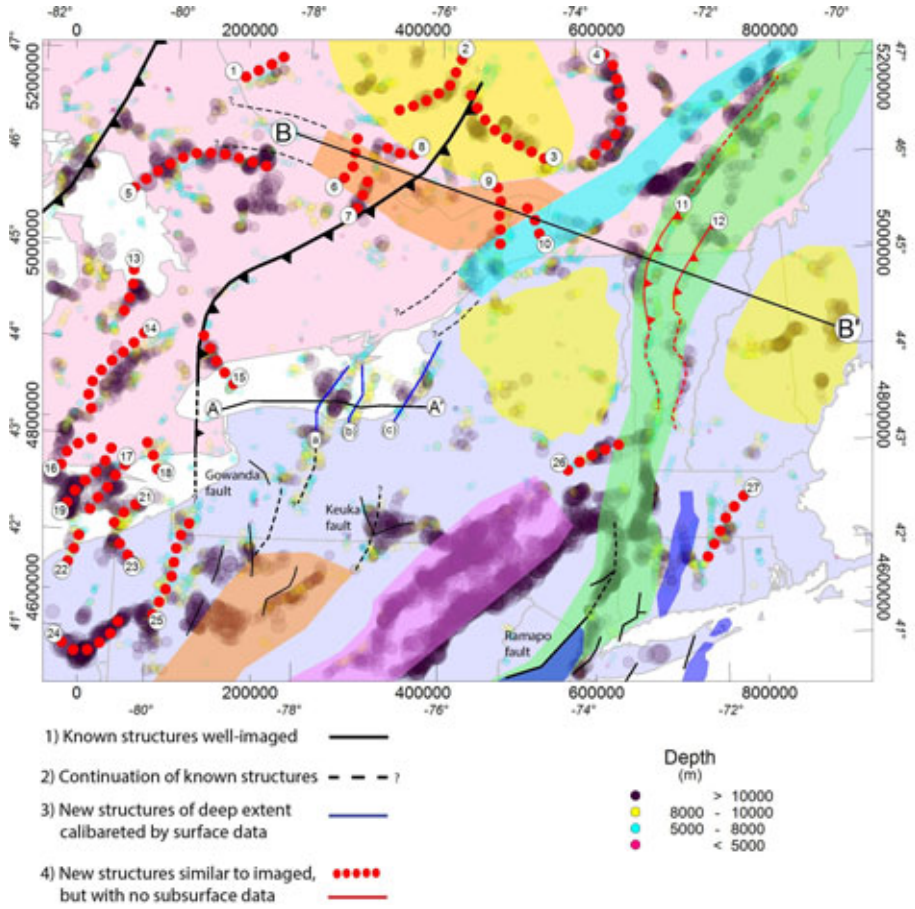

Figure 21. Overlay of tectonic zones shown in Figure 3b on a map of the most contiguous in length and depth of the Euler solutions. We have done the same with the worms, but the diagram is cluttered. Numbers refer to previously mapped faults (with sense of offset), and structures interpreted in this study (Navarrete, 2015). A, b, c are shallow faults explained in text and Figure SM3.

Cross Section B-B' (Supplementary Material) crosses the Grenville Metasedimentary belt, the upper St. Lawrence rift, the northern Adirondack block, northern Appalachians, Green Mountains (thrust 12) and White Mountains intrusives, and illustrates crustal structure within these areas. Specifically, Euler deconvolution and 'worm' results reveal steep structures that also agree with the velocity model constraints from *Musacchio et al.* (1997) and *Hughes & Luetgert* (1991,1992). In particular, we observe solutions from both of our inverse methods that coincide with the velocity model's major lateral velocity change in the upper and middle crust interpreted as the Grenville Ramp dividing the Grenville Province and Appalachian Province (Figure 21, SM4). In particular, solutions correlating with the Grenville Ramp and nearby sub-parallel solutions can be connected to the locations of the Champlain thrust and Eden Notch fault system (*Mereu et al.* 1986)(11, 12 on Figure 21). The high-density mid-crustal anorthosite Tahawus complex presented in *Musacchio et al.* (1997) and *Hughes & Luetgert* (1991,1992) is required to explain the local gravity anomaly high located at the middle of Profile B-B' (Fig. SM4). This implies the Tahawus complex extends laterally beyond the current geologic map boundaries of the Adirondack Mountains. The magnetic worm results reveal steep pipe-like bodies stemming from the Tahawus complex, possibly indicating a conduit feeding the Tahawus complex.

6.3 ECC-AM

Although at the edge of our study region, N-S and NNE-striking lineaments correlate with known large offset normal faults and mafic intrusives of the Mesozoic rift system. Examples are the border faults to the Hartford basin in Connecticut, the Ramapo fault in New York and New Jersey, and structures beneath Long Island (Fig. 21). Further detailed analyses in smaller areas is needed to calibrate and compare crustal seismic, well, and other data sets from the ECC-AM and continental shelf regions.

6.4 PEZ-W

Our inversion results and predictive models for the crustal structure of Lake Ontario largely reflect the crustal structure of the Central Metasedimentary Belt of the Grenville province. The area west of 78°W is characterized by NNE-striking solutions. The most profound in terms of gradients and depth extent is the Grenville front, which we can map beneath Georgian bay. Solutions characterize only some sectors of the Central Metasedimentary Belt Boundary Zone (CMBBZ), large thrusts mapped at the surface in Canada (Figs. 2, 3, 21). We suggest that the CMBBZ continues beneath western Lake Ontario and eastern Lake Erie (7, Figure 21). We also identify several other prominent and coincident gravity and magnetic anomalies with Euler and worm solutions of crustal extent in the western part of the study area. Given their NE trend, they are most likely Grenville thrust contacts.

One of our focus areas for calibration and interpretation is the NNE-trending anomalies traversing Lake Ontario that are well imaged along the vintage seismic profile of *Forsyth et al.* (1994a). Receiver functions reveal complex crustal lamination (double peak at station J55A, Figure 11B), which we interpret as a magmatic underplate. Two strong reflectors observed at 37 and 49 km depth subsurface suggest a zone of higher density crust lying above mantle lithosphere. However, crustal thickness variations alone could not reproduce observed gravity anomalies, and density anomalies throughout the crust are required to match the observed wavelength and amplitudes. Eastward-dipping reflections interpreted as westward-verging thrust sheets are imaged in the 1971 reflection profile (*Forsyth et al., 1994a*). The Paleozoic-Recent sedimentary strata overlying metamorphic basement are ~5 km thick, almost twice the mean thickness along the seismic profile.

Potential fields results indicate that this thick sedimentary sequence is bounded on its west and east by a system of NNE-striking faults that are steep at the surface, and sub-parallel to the Proterozoic Rome Trough faults in western Pennsylvania and West Virginia (Fig. 21). We call this basin the Rochester basin because the eastern fault zone passes through the greater Rochester area (*Navarrete*, 2015). The surface expression of the east-dipping faults bounding the basin are on-strike projections of the Scotch Bonnet Rise and the Point-Petre ridge beneath Lake Ontario, two prominent bathymetric figures that show evidence of surface breaks in some areas (*Jacobi et al.,* 2007; *Navarrete,* 2015). We call the westernmost fault the Manitou fault, and the easternmost fault the Point Petre fault (a, b on Figure 21). A third fault that extends from the surface to lower crustal levels is the NNE-striking Carthage-Colton fault zone, a mylonite at the surface (*Forsyth et al.* 1994a) (c on Figure 21).

Cross Section A-A' (Figure SM3) illustrates many of the known structures that are well imaged, and reveals several more structures that penetrate to lower crustal levels. The NNE-strike of the Manitou and Point Petre faults, as well as the receiver function suggest mafic additions to the lower crust beneath the Rochester basin, and a possible rift origin. No well data are available to date the age of sedimentary strata beneath surface outcrops of Paleozoic age (Forsyth, 1994a), but the parallelism of faults, and the geographic location suggests that these new crustal scale faults beneath Lake Ontario are a northward continuation of the Rome Trough rift system. The arcuate reflection patterns in the reflection seismic data and our inverse method results suggest a series of imbricate west-verging thrusts of varying composition underlie the Appalachian basin in northwestern New York State. The aligned Euler and worm solutions pass through Mesozoic kimberlite intrusions in the Finger Lakes region (Keuka fault zone, Fig. 21), suggesting that some of the anomalies are caused by magmatic intrusives at mid-crustal depths .

6.5 Steep Crustal Boundaries and Seismicity

Comparisons of our new, calibrated steep crustal density and magnetic susceptibility contrasts throughout Northeast North America reveal a spatial correlation between the location of interpreted steep structures and seismicity (Figures 20, 21). With specific reference to earthquake hazards in New England, Over 20% of the well-located earthquakes are coincident with gravity and magnetic inverse models. Specific examples are well-imaged structures beneath the two sub-parallel bands of earthquakes in the Charlevoix region as outlined by *Mazzotti & Townend* (2010) (Figs. 15, 21). New crustal-scale faults calibrated from reflection data beneath Lake Ontario and mapped southward through the greater Rochester urban center

near the Ginna nuclear reactor are also favorably oriented in terms of the tectonic stress (Figs. 20, 21).

7. Recommendations

In order to further focus attention on re-activation of pre-existing structures, we suggest that the co-occurrence of TA located seismicity, regional scale faults identified with potential fields methods, and population centers or other high-risk sites should be subject to a higher level of scrutiny. This strategy has the potential to alter the currently known seismic hazard risks by adding previously unrecognized hazards to the maps, and better constraining crustal structure regionally. Additional, full-state-of-stress information nearby to populations and infrastructure at risk would greatly improve the risk estimates of the class shown in Figures 23 a) and b). Knowledge of the location and orientation of large basement structures provides a foundation for probabalistic models of stress triggering in the Eastern US. As mantle tomography and lithosphere-asthenosphere mapping studies with new EarthScope data sets are completed, our crustal studies will offer important clues into causative mechanisms for intraplate earthquakes.

8. Conclusions

Our systematic analyses of regional gravity and magnetic data using two spectral estimation techniques reveals crustal-scale contacts and structures, many of which can be calibrated with structures mapped at the surface or from multiple seismic methods and magnetotelluric data. Although the comparison of methods and theory indicate that the dip of structures is weakly constrained, many of the interpreted structures are seismogenic. Given that much of the study region used in the statistical comparison of potential faults and earthquake hypocenters is aseismic (including the Canadian shield), more detailed comparisons of structures and seismicity should be undertaken in the seismogenic zones. Although in no way proof that lateral density contrasts localize strain in continental interiors, nearly all of the clustered seismicity occurs on or near structures of large lateral and depth extent delineated in our studies. Many other structures separating crust of different composition, such as the CMBBZ, are apparently aseismic. Clearly, this style of work has the potential to identify seismically at-risk geological structures in regions other than the one we studied, being primarily based on widely available gravity and magnetic regional datasets, regional seismicity studies, and globally available foundations such as the World Stress Map.

Below we list results common to multi-scale wavelet and Euler deconvolution models of Bouguer gravity, magnetic, and pseudo-gravity anomalies.

8.1 Regional

- Euler and wavelet solutions coincide, but the Poisson wavelet method provides better spatial resolution
- Within the Grenville Province, Ottawa-Bonnechère-St. Lawrence rift systems, Appalachian Belt and basin, and Mesozoic basins, some Euler and Poisson wavelet solutions coincide known structures
- Where no subsurface data exist, locations where Euler and Poisson wavelet solutions coincide are interpreted as new deep structures
- Deep structure has a robust spatial correlation with seismicity, suggesting that steep lateral density contrasts localize intraplate stresses.
- Long, deep potential fields solutions lying within proximity to population and infrastructure should be prioritized for future detailed studies. An example is the fault-bounded basin beneath Lake Ontario where faults pass within <20 km of an aging nuclear plant near Rochester.

8.2 Area-Specific results.

Northern Appalachians

- Within Appalachian belt we image two deep structures that can be connected to the locations of the Champlain thrust and Eden Notch fault system.
- Our predictive model requires a high density mid-crustal body, supporting the interpretation of the Tahawus complex of Musacchio et al. (1997) and Hughes and Luetgert (1991,1992)

Paleozoic Extended Province (Lake Ontario focus site)

- Euler deconvolution and worms reveal deep structure on the eastern side of Lake Ontario. We interpret this structure as the continuation of the Carthage-Colton mylonite zone (c on Figure 21)
- All models suggest the Grenville front extends beneath western Lake Ontario and beneath Lake Erie to a zone of re-injection wells in Ohio (Kim et al., 2013)
- Forward models constrained by Euler gravity and magnetic anomaly solutions, along with seismic reflection, and receiver functions reveal that the gravity low through the center of Lake Ontario is a fault bounded sedimentary basins underlain by unusual, possibly underplated crust.

References

Adams, J., and Basham, P.W. (1991).The seismicity and seismotectonics of eastern Canada, *in* Slemmon, B., et al., eds., The Geology of North America, Decade Map Volume 1, Neotectonics of North America: Boulder, Colorado, Geological Society of America, p. 261–276.

Bahavar, M. and Trabant, C. (2010) EarthScope Automated Receiver Survey (EARS) at the IRIS DMC , *IRIS Data Services Newsletter*, **12**, 2.

Benoit, M. H., Ebinger, C., & Crampton, M. (2014). Orogenic bending around a rigid Proterozoic magmatic rift beneath the Central Appalachian Mountains. *Earth and Planetary Science Letters*.

Blakely, R. J. (1996). *Potential theory in gravity and magnetic applications*. Cambridge University Press.

Boschetti, F., Hornby, P., & Horowitz, F. G. (2001). Wavelet Based Inversion of Gravity Data. *Exploration Geophysics*, *32,* (1), 48-55. URL http://dx.doi.org/10.1071/EG01048

Brocher, T. M. (2005). Empirical relations between elastic wavespeeds and density in the Earth's crust. *Bulletin of the Seismological Society of America*, *95*(6), 2081-2092.

Brown L., C. Ando, S. Klemperer, J. Oliver, S. Kaufman, B. Czuchra, T. Walsh and Y.W. Isachsen, Adirondack-Appalachian crustal structure: The COCORP Northeast traverse. *GSA Bull.*, **94**, 1173-1184, 1983.

Bürgmann, R., & Dresen, G. (2008). Rheology of the lower crust and upper mantle: Evidence from rock mechanics, geodesy, and field observations. *Annual Review of Earth and Planetary Sciences*, *36*(1), 531.

Byerlee, J. (1978). Friction of rocks. Pure and Applied Geophysics, 116 (4-5), 615-626. URL http://dx.doi.org/10.1007/bf00876528

Carpenter, K., Horowitz, F. G., Ebinger, C., Navarrete, L., & Diaz-Etchevehere, D. (2015). Identifying active faults in Northeast North America using hypocenters and multiscale edge wavelet analyses of potential fields. In 2015 Fall Meeting, (pp. T11A-2866+). American Geophysical Union.

CEUS-SSC (2012). Central and Eastern United States seismic source characterization for nuclear facilities. Tech. rep., EPRI, Palo Alto, CA; U.S. DOE; U.S. NRC. URL http://www.ceus-ssc.com/PDF/CEUS_SSC_Report.zip

Connerney J.E.P., A.F. Kuckes, Gradient analysis of geomagnetic fluctuations in the Adirondacks. *J. Geophys. Res.*, **85**, 2615-2624, 1980.

Crough, S.T., Mesozoic hotspot epeirogeny in eastern North America. *Geology*, **9**(1), 2-6, 1981.

Eaton, D., J. Adams, I. Asudeh, G. Atkinson, M. Bostock, J. Cassidy, I. Ferguson, C. Samson, D. Snyder, K. Tiampo, and M. Unsworth, Investigating Canada's lithosphere and earthquake hazards with portable arrays. *EOS Trans. AGU,* **86**, 169-173, 2005.

Eaton, D., and A. Frederiksen, Seismic evidence for convection-driven motion of the North American plate. *Nature,* **446**, 428–431, 2007.

Ebel, J.E., and M. Tuttle, Earthquakes in the Eastern Great Lakes Basin from a regional perspective. *Tectonophysics*, **353**, 17-30, 2002.

Ellsworth, William L. "Injection-induced earthquakes." *Science* 341, no. 6142 (2013): 1225942.

Forsyth, D. A., Milkereit, B., Zelt, C. A., White, D. J., Easton, R. M., & Hutchinson, D. R. (1994a). Deep structure beneath Lake Ontario: crustal-scale Grenville subdivisions. *Canadian Journal of Earth Sciences*, *31*(2), 255-270.

Forsyth, D. A., Milkereit, B., Davidson, A., Hanmer, S., Hutchinson, D. R., Hinze, W. J., & Mereu, R. F. (1994b). Seismic images of a tectonic subdivision of the Grenville Orogen beneath lakes Ontario and Erie. *Canadian Journal of Earth Sciences*, *31*(2), 229-242.

Freed, A. M. (2005). Earthquake triggering by static, dynamic, and postseismic stress transfer. *Annu. Rev. Earth Planet. Sci.*, *33*, 335-367.

GoldCorp (2001). US$575,000 goldcorp challenge awards world's first 6 million ounce internet gold rush yields high grade results! Press Release. URL http://www.infomine.com/index/pr/Pa065434.PDF

Hatcher, R. D. (2010). The Appalachian orogen: A brief summary. *Geological Society of America Memoirs*, *206*, 1-19.

Heaman, L.M. and B.A. Kjarsgaard, Timing of eastern North American kimberlite magmatism: continental extension of the Great Meteor hotspot track? *Earth Planet Sci. Lett.,* **178**(3-4), 253–268, 2010.

Heidbach, O., Tingay, M., Barth, A., Reinecker, J., Kurfeß, D., & Müller, B. (2010). Global crustal stress pattern based on the World Stress Map database release 2008. Tectonophysics, 482 (1-4), 3-15. URL http://dx.doi.org/10.1016/j.tecto.2009.07.023

Hildenbrand, T.G., Briesacher, A., Flanagan, G., Hinze, W. J., Hittelman, A. M., Keller, G. R., Kucks, R. P., Plouff D., Roest W., Steeley J., Smith D.A., & Webring, M. (2002). *Rationale and operational plan to upgrade the US gravity database*. US Department of the Interior, US Geological Survey.

Hinze, W. J., Aiken, C., Brozena, J., Coakley, B., Dater, D., Flanagan, G., Forsberg R., Hildenbrand T., Keller G., Kellogg J., Kucks R., Li X., Mainville A., Morin R., Pilkington M., Plouff D., Ravat D., Roman D., Urrutia-Fucugauchi J., Veronneau M., Webring M., & Winester, D. (2005). New standards for reducing gravity data: The North American gravity database. *Geophysics*, *70*(4), J25-J32.

Hornby, P., Boschetti, F., & Horowitz, F. G. (1999). Analysis of potential field data in the wavelet domain. *Geophysical Journal International*, *137*(1), 175-196.

Hornby, P., Horowitz, F. G., & Boschetti, F. (2002). A physical interpretation of the Poisson wavelet transform of potential fields. In *EGS General Assembly Conference Abstracts,* v. 27, p. 5568).

Horowitz, F. G., & Gaede, O. (2014). BSDWormer; an open source implementation of a Poisson wavelet multiscale analysis for potential fields. In 2014 Fall Meeting, T43C-4743. American Geophysical Union. URL http://abstractsearch.agu.org/meetings/2014/FM/T43C-4743.html

Horowitz, F. G., & the Appalachian Basin Geothermal Play Fairway Analysis Team (2016). Risk of seismicity from potential direct-use operations in the Appalachian Basin geothermal play fairway project. In 41st Annual Stanford Geothermal Workshop. Stanford University. URL https://pangea.stanford.edu/ERE/db/GeoConf/papers/SGW/2016/Horowitz.pdf

Hughes, S., & Luetgert, J. H. (1991). Crustal structure of the western New England Appalachians and the Adirondack Mountains. *Journal of Geophysical Research: Solid Earth (1978–2012)*, *96*(B10), 16471-16494.

Hughes, S., & Luetgert, J. H. (1992). Crustal structure of the southeastern Grenville Province, northern New York State and eastern Ontario. *Journal of Geophysical Research: Solid Earth (1978–2012)*, *97*(B12), 17455-17479.

Isachsen, Y. W., Possible evidence for contemporary doming of the Adirondack mountains, New York, and suggested implications for regional tectonics and seismicity, *Tectonophysics*, **29**, 169-181, 1975.

Isachsen, Y.W., Contemporary doming of the Adirondack mountains: Further evidence from relevleing. *Tectonophysics*, **71**, 95-96, 1981.

Isachsen, Y.W., and W.M. Kelley, Still rising after all these years. *Natural History Magazine*, **101**, 30-34, 1992.

Jacobi, R. D. (2002). Basement faults and seismicity in the Appalachian Basin of New York State. *Tectonophysics*, *353*(1), 75-113.

Jacobi, R.D., C.F.M. Lewis, Q. Zhang, E. Sandvol (2007). Popup field in Lake Ontario south of Toronto, Canada: Indicators of late glacial and postglacial strain, in S. Stein and S. Mazzotti, *Continental Intraplate Earthquakes: Science, Hazard and Policy Issues*, Geol Soc. Spec. Pub., 425, pp. 129-148.

Kent, D. V., B. A. Kjarsgaard, J. S. Gee, G. Muttoni, and L. M. Heaman (2015), Tracking the Late Jurassic apparent (or true) polar shift in U-Pb-dated kimberlites from cratonic North America (Superior Province of Canada), *Geochem. Geophys. Geosyst*., 16, 983–994, doi:10.1002/2015GC005734.

Kim, W. Y. (2013). Induced seismicity associated with fluid injection into a deep well in Youngstown, Ohio. *Journal of Geophysical Research: Solid Earth*, *118*(7), 3506-3518.

King, G. C., Stein, R. S., & Lin, J. (1994). Static stress changes and the triggering of earthquakes. *Bulletin of the Seismological Society of America*, *84*(3), 935-953.

Kumarapeli, P. S., & Saull, V. A. (1966). The St. Lawrence valley system: a North American equivalent

of the East African rift valley system. *Canadian Journal of Earth Sciences*, *3*(5), 639-658.

Kusznir, N. J., & Park, R. G. (1987). The extensional strength of the continental lithosphere: its dependence on geothermal gradient, and crustal composition and thickness. *Geological Society, London, Special Publications*, *28*(1), 35-52.

Levin, V., Lerner‐Lam, A., & Menke, W. (1995). Anomalous mantle structure at the Proterozoic‐Paleozoic boundary in northeastern US. *Geophysical research letters*, *22*(2), 121-124.

Lowry, A. R., & Pérez-Gussinyé, M. (2011). The role of crustal quartz in controlling Cordilleran deformation. Nature, 471 (7338), 353-357.

Ma, S. and D.W. Eaton, Western Quebec Seismic Zone (Canada): Clustered, mid-crustal seismicity along a Mesozoic hotspot track. *J. Geophys. Res.,* 112, B06305, doi:10.1029/2006JB004827, 2007.

Ma, S., D.W. Eaton, and J. Adams, Intraplate seismicity of a recently deglaciated shield terrane: A case study from northern Ontario, Canada. *Bull. Seis. Soc. Am.,* 98, 2828-2848, 2008.

Mardia, K. V. (1972). Statistics of directional data. Academic Press.

Mazzotti, S., T.S. J. Henton and J. Adams, GPS crustal strain, postglacial rebound, and seismic hazard in eastern North America: The Saint Lawrence valley example. *J. Geophys. Res.,* 110, B11301, doi: 10.1029/2004JB003590, 2005.

Mazzotti, S., & Townend, J. (2010). State of stress in central and eastern North American seismic zones. *Lithosphere*, *2*(2), 76-83.

McLelland, J. M., Selleck, B. W., & Bickford, M. E. (2010). Review of the Proterozoic evolution of the Grenville Province, its Adirondack outlier, and the Mesoproterozoic inliers of the Appalachians. *Geological Society of America Memoirs*, *206*, 21-49.

Mereu, R. F., Wang, D., Kuhn, O., Forsyth, D. A., Green, A. G., Morel, P., ... & Clowes, R. (1986). The 1982 COCRUST seismic experiment across the Ottawa–Bonnechere graben and Grenville Front in Ontario and Quebec. *Geophysical Journal International*, *84*(3), 491-514.

Moreau, F., Gibert, D., Holschneider, M., & Saracco, G. (1997). Wavelet Analysis of Potential Fields. Inverse Problems, 13 , 165-178. URL http://dx.doi.org/10.1088/0266-5611/13/1/013

Muir, T.L. 2013. Ontario Precambrian bedrock magnetic susceptibility geodatabase for 2001 to 2012; Ontario Geological Survey, Miscellaneous Release—Data 273 – Revised.

Musacchio, G., Mooney, W. D., Luetgert, J. H., & Christensen, N. I. (1997). Composition of the crust in the Grenville and Appalachian Provinces of North America inferred from Vp/Vs ratios. *Journal of Geophysical Research: Solid Earth (1978–2012)*, *102*(B7), 15225-15241.

National Research Council (US). Committee on Induced Seismicity Potential in Energy Technologies, 2013. *Induced Seismicity Potential in Energy Technologies,* National Academies Press, 248p.

National Geophysical Data Center, 1999. Bathymetry of Lake Ontario. National Geophysical Data Center, NOAA. doi:10.7289/V56H4FBH [April 2014].

Navarrete, L. (2015). Crustal structure of NE N. America from constrained models of potential field data.. Master's thesis, University of Rochester.

Newman, A., Stein, S., Weber, J., Engeln, J., Mao, A., & Dixon, T. (1999). Slow deformation and lower seismic hazard at the New Madrid seismic zone. *Science*, *284*(5414), 619-621.

Petit, C. and C. Ebinger, Flexure and mechanical behavior of cratonic lithosphere: Gravity models of the East African and Baikal rifts. *J. Geophys. Res.,* 105(B8), 19,151–19,162, 2000.

Ratcliffe, N.M., Stanley, R.S., Gale, M.H., Thompson, P.J., and Walsh, G.J. (2011). Bedrock geologic map of the Vermont: U. S. Geological Survey Scientific Investigations Map 3184, scale 1:100,000.

Ravat, D., Sabaka, T., Elshayat, A., Aref, A., Elawadi, E., Kucks, R., ... & Blakely, R. J. (2008, December). A preliminary full spectrum magnetic anomaly database of the United States with improved long wavelengths for studying continental dynamics. In *AGU Fall Meeting Abstracts* (Vol. 1, p. 02).

Ravat, D., Finn, C., Hill, P., Kucks, R., Phillips, J., Blakely, R., Bouligand, C., Sabaka, T., Elshayat, A., Aref, A., & Elawadi, E. (2009). A Preliminary, Full Spectrum, Magnetic Anomaly Grid of the United States with Improved Long Wavelengths for Studying Continental Dynamics: A Website for Distribution of Data. Open-File Report 2009–1258. USGS. URL http://pubs.usgs.gov/of/2009/1258/

Reid, A. B., Allsop, J. M., Granser, H., Millett, A. J., & Somerton, I. W. (1990). Magnetic interpretation in three dimensions using Euler deconvolution. *Geophysics*, *55*(1), 80-91.

Rondenay, S., M. Bostock, T. Hearn, D. White, and R. Ellis, Lithospheric assembly and modification of the SE Canadian Shield: Abitibi-Grenville teleseismic experiment. *J. Geophys. Res*. **105**, 13,735–13,755, 2000.

Schlische, R. W., Withjack, M. O., & Olsen, P. E. (2003). Relative timing of CAMP, rifting, continental breakup, and basin inversion: tectonic significance. *The Central Atlantic Magmatic Province: Insights from Fragments of Pangea*, 33-59.

Sella, G. F., Stein, S., Dixon, T. H., Craymer, M., James, T. S., Mazzotti, S., & Dokka, R. K. (2007). Observation of glacial isostatic adjustment in "stable" North America with GPS. *Geophysical Research Letters*, *34*(2).

Selleck, B. W., McLelland, J. M., & Bickford, M. E. (2005). Granite emplacement during tectonic exhumation: The Adirondack example. *Geology*, *33*(10), 781-784.

Sleep, N. H. (1990). Hotspots and mantle plumes: Some phenomenology. *Journal of Geophysical Research: Solid Earth (1978–2012)*, *95*(B5), 6715-6736.

Smalley, R., Ellis, M. A., Paul, J., & Van Arsdale, R. B. (2005). Space geodetic evidence for rapid strain rates in the New Madrid seismic zone of central USA. *Nature*, *435*(7045), 1088-1090.

Tremblay, A., Long, B., & Massé, M. (2003). Supracrustal faults of the St. Lawrence rift system, Québec: kinematics and geometry as revealed by field mapping and marine seismic reflection data. Tectonophysics, 369(3), 231-252

van der Elst, N.J., Savage, H.M., Keranen, K.M. and Abers, G.A., 2013. Enhanced remote earthquake triggering at fluid-injection sites in the midwestern United States. *Science*, *341*(6142), pp.164-167.

Villemaire, M., Darbyshire, F. A., & Bastow, I. D. (2012). P-wave tomography of eastern North America: Evidence for mantle evolution from Archean to Phanerozoic, and modification during subsequent hot spot tectonism. *J. Geophys. Res.,* 117(B12).

Vlahovic, G., Powell, C., and Lamontagne, M. (2003). A three- dimensional P wave velocity model for the Charlevoix seismic zone, Quebec, Canada: Journal of Geophysical Research, v. 108, no. B9, p. 2439, doi: 10.1029/ 2002JB002188.

Whitmeyer, S. J., & Karlstrom, K. E. (2007). Tectonic model for the Proterozoic growth of North America. *Geosphere*, *3*(4), 220-259.

Winardhi, S., & Mereu, R. F. (1997). Crustal velocity structure of the Superior and Grenville provinces of the southeastern Canadian Shield. *Canadian Journal of Earth Sciences*, *34*(8), 1167-1184.

Withjack, M. O., Schlische, R. W., & Olsen, P. E. (1998). Diachronous rifting, drifting, and inversion on the passive margin of central eastern North America: an analog for other passive margins. *AAPG bulletin*, *82*(5), 817-835.

Wong, M. S., Williams, M. L., McLelland, J. M., Jercinovik, M. J., & Kowalkoski, J. (2012). Late Ottawan extension in the eastern Adirondack Highlands: Evidence from structural studies and zircon and monazite geochronology. *Geological Society of America Bulletin*, *124*(5-6), 857-869.

Supplementary Material

Table SM1. References to seismic data sets referred to by numbers in Figure 5.

#	Citation	#	Citation
1	Ando, C. J., Cook, F. A., Oliver, J. E., Brown, L. D., & Kaufman, S. (1983). Crustal geometry of the Appalachian orogen from seismic reflection studies. *Geological Society of America Memoirs ,158* , 83-102.	11	Mereu, R. F., Wang, D., Kuhn, O., Forsyth, D. A., Green, A. G., Morel, P., ... & Clowes, R. (1986). The 1982 COCRUST seismic experiment across the Ottawa–Bonnechere graben and Grenville Front in Ontario and Quebec. *Geophysical Journal International ,84* (3), 491-514.
2	Ando, C. J., Czuchra, B. L., Klemperer, S. L., Brown, L. D., Cheadle, M. J., Cook, F. A., ... & Rosenfeld, J. L. (1984). Crustal profile of mountain belt: COCORP deep seismic reflection profiling in New England Appalachians and implications for architecture of convergent mountain chains. *AAPG Bulletin ,68* (7), 819-837.	12	Mereu, R. F. (2000). The complexity of the crust and Moho under the southeastern Superior and Grenville provinces of the Canadian Shield from seismic refraction-wide-angle reflection data. *Canadian Journal of Earth Sciences ,37* (2-3), 439-458.
3	Asudeh, I., Forsyth, D., Mortimer, D., Argyle, M., Zelt, C., Mereu, R., ... & Jessop, J. (1993). *1992 Lithoprobe Abitibi-Grenville Seismic Refraction Survey: Acquisition and Processing Report* . University of British Columbia, Lithoprobe secretariat.	13	Ouassaa, K., & Forsyth, D. A. (2002). Interpretation of seismic and potential field data from western New York State and Lake Ontario. *Tectonophysics ,353* (1), 115-149.
4	Braile, L. W., Hinze, W. J., Von Frese, R. R. B., & Keller, G. R. (1989). Seismic properties of the crust and uppermost mantle of the conterminous United States and adjacent Canada. *Geological Society of America Memoirs ,172* , 655-680.	14	Ouassaa, R., Forsyth, D. , & White, D. (2002). The 2000 southern Ontario seismic project. *Geological Survey of Canada, Ottawa*, in Current Research, 2002-E9, 9 pp.
5	Brown, L., Ando, C., Klemperer, S., Oliver, J., Kaufman, S., Czuchra, B., ... & Isachsen, Y. W. (1983). Adirondack-Appalachian crustal structure: the COCORP northeast traver	15	Phinney, R. A., & Roy-Chowdhury, K. (1989). Reflection seismic studies of crustal structure in the eastern United States. *Geological Society of America Memoirs ,172* , 613-624.
6	Hodgson, J. H. (1953). A Seismic Survey in the Canadian Shield I: Refraction Studies Based on Rockbursts at Kirkland Lake, Ont. Queen's Printer.	16	Taylor, S. R., & Toksandoumlz, M. N. (1982). Structure in the northeastern United States from inversion of Rayleigh wave phase and group velocities. *Seismological Research Letters ,53* (4), 5-24.
7	Katz, S. (1955). Seismic study of crustal structure in Pennsylvania and New York. *Bulletin of the Seismological Society of America ,45* (4), 303-325.	17	Taylor, S. R., & Toksöz, M. N. (1979). Three-dimensional crust and upper mantle structure of the northeastern United States. *Journal of Geophysical Research: Solid Earth (1978–2012) ,84* (B13), 7627-7644.
9	Klemperer, S. L., Brown, L. D., Oliver, J. E., Ando, C. J., Czuchra, B. L., & Kaufman, S. (1985). Some results of COCORP seismic reflection profiling in the Grenville-age Adirondack Mountains, New York State. *Canadian Journal of Earth Sciences ,22* (2), 141-153.	18	Taylor, S. R., Toksöz, M. N., & Chaplin, M. P. (1980). Crustal structure of the northeastern United States: contrasts between Grenville and Appalachian Provinces. *Science ,208* (4444), 595-597.
10	Ludden, J., & Hynes, A. (2000). The Lithoprobe Abitibi-Grenville transect: two billion years of crust formation and recycling in the Precambrian Shield of Canada. *Canadian Journal of Earth Sciences ,37* (2-3), 459-476.	19	Zelt, C. A., Forsyth, D. A., Milkereit, B., White, D. J., Asudeh, I., & Easton, R. M. (1994). Seismic structure of the Central Metasedimentary belt, southern Grenville province. *Canadian Journal of Earth Sciences ,31* (2), 243-254.

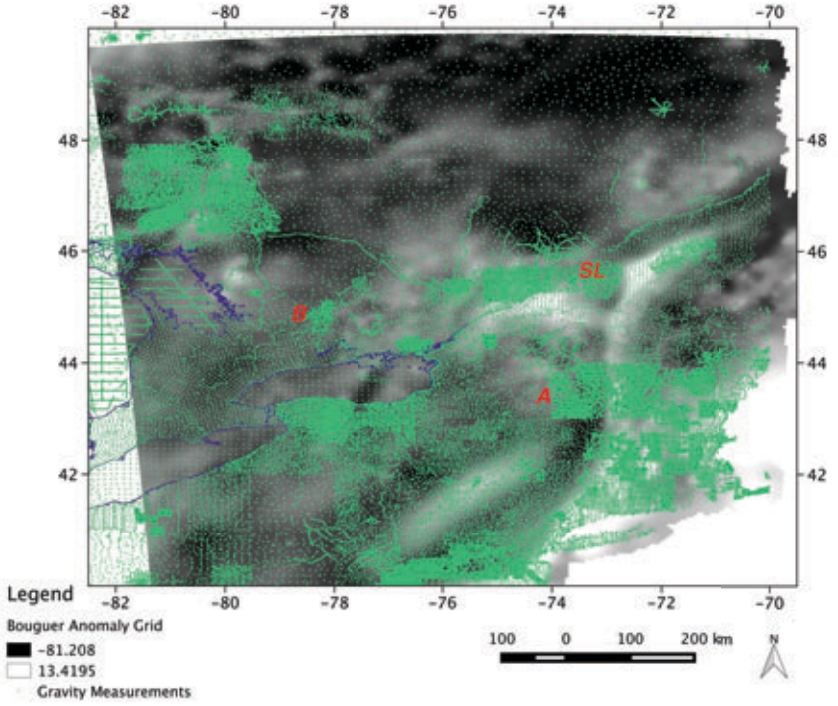

Figure SM1. Gravity data points on Bouguer gravity anomaly values, as in Figure 8.

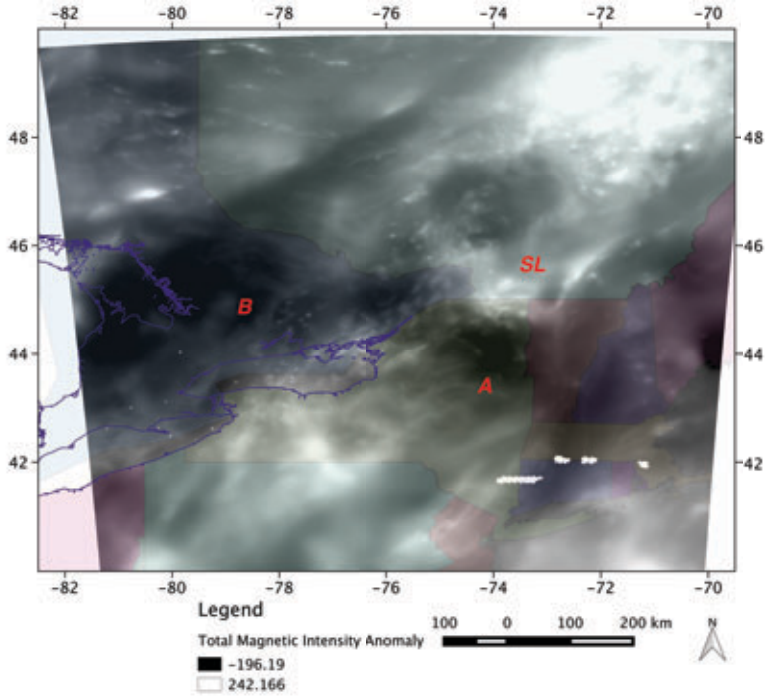

Figure SM2. Pseudogravity anomaly map (PGA) used in wavelet-based analyses. We transform magnetic anomalies to pseudo-gravity (monopole) anomalies (e.g. *Blakely*, 1996; equivalent to reduced to pole total field magnetic anomalies followed by vertical integration then scaled to gravity amplitudes) prior to wavelet analyses to enable direct comparison with gravity anomaly solutions.

Figure SM3: Lake Ontario predictive model. Magnetic anomalies (top); Bouguer gravity anomalies (middle), and simplified geologic cross section (bottom) constrained by receiver function estimates of crustal thickness, Euler deconvolution solutions defining steep density and magnetic susceptibility contrasts, and seismic reflection survey. Manitou fault and Point Petre fault bound the west and east edges of the Ontario sedimentary basin, respectively. Line of section is shown on Figure 11, and Figure 21.

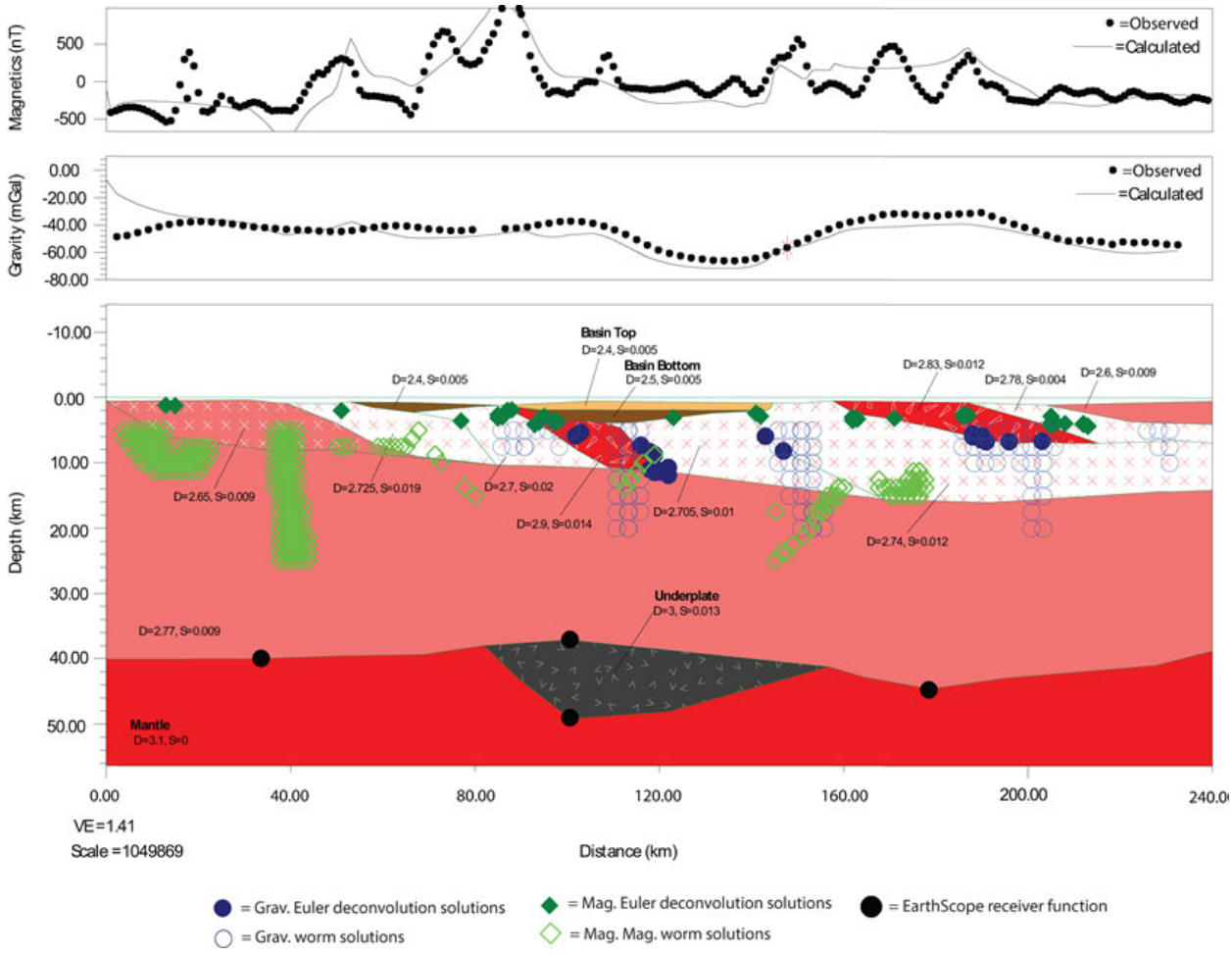

Figure SM4. Comparison of predicted and observed Bouguer anomaly (top) from a geological model of lateral boundaries in rock density and magnetic susceptibility along a transect of the upper St. Lawrence rift zone and Adirondack Mts (bottom). Crustal thickness and contacts are constrained by EarthScope receiver functions and controlled source seismic (Musacchio et al., 1997). Density estimated from Vp velocity following empirical relations of Brocher (2005). Hollow circles and diamonds are locations of Poisson wavelet multi-scale edges worms. 'Grenville Ramp' interpreted location is marked by black line separating the Grenville and Appalachian province. Tahawus complex, a dense anorthosite body, is indicated by a white background with red triangles and density of 2.95 g/cm3. Line of section is show on figure 11A as B-B'.